

Student thesis series INES nr 473

UAV based hyperspectral grassland monitoring in an alpine shallow erosion area

Lessons learnt from classifying vegetation
indicating shallow erosion risk

John Lloyd Peitz

2019
Department of
Physical Geography and Ecosystem Science
Lund University
Sölvegatan 12
S-223 62 Lund
Sweden



John Lloyd Peitz (2019).

***UAV based hyperspectral grassland
monitoring in an alpine shallow erosion area***

Master degree thesis, 30 credits in *Geomatics*

Department of Physical Geography and Ecosystem Science, Lund University

Level: Master of Science (MSc)

Course duration: *September 2018* until *June 2019*

Disclaimer

This document describes work undertaken as part of a program of study at the University of Lund. All views and opinions expressed herein remain the sole responsibility of the author, and do not necessarily represent those of the institute.

UAV based hyperspectral grassland monitoring in an alpine shallow erosion area

Lessons learnt from classifying vegetation indicating
shallow erosion risk

John Lloyd Peitz

Master thesis, 30 credits, in the Master's Programme of Geomatics

Supervisors:

Abraham Mejia Aguilar, Ph.D, Eurac Research

&

Virginia Garcia-Millan, Ph.D, Lund University

Examiners:

Frans-Jan Parmentier, Ph.D, Lund University

Per-Ola Olsson, Ph.D, Lund University

John L. Peitz

UAV based hyperspectral grassland monitoring in an alpine shallow erosion area

Recent research in the Alps found that a reduction in grassland management is correlated to an increase in a certain type of shallow erosion areas called blaiken. This change also entails changes to the dominant grassland vegetation. New developments in hyperspectral technology have produced cameras which are sufficiently light for Unmanned Aerial Vehicles (UAVs). This thesis explores whether UAV mounted hyperspectral cameras (RIKOLA (SENOP Optronics, Lievestuore, Finland)) can detect the spectral signatures of managed vs. blaiken-related unmanaged grasslands accurately, and whether their signatures are so distinct as to enable grassland classification on an aerial image. Accurate mapping of Alpine grasslands can guide erosion mitigation measures to manage grassland types that are more susceptible to erosion.

A field study was undertaken at a blaiken hotspot at the Schlüter lodge, located in the Dolomite mountain range within the Italian Alps, in order to evaluate the accuracy of the RIKOLA camera. Its spectral signatures taken on the ground were compared to those of a high precision spectroradiometer (Spectra Vista Corporation, Poughkeepsie, USA). The study also evaluates whether the spectral signatures of different grassland types were sufficiently unique and the quality of the Rikola images taken from the UAV system was high enough to permit the characterization of grassland types by a maximum likelihood classification algorithm.

The spectral separability analysis demonstrated that the spectral signatures of designated grassland classes separate in Rikola images taken on the ground. However, an orthomosaic created from aerial UAV-Rikola images displayed low precision and accuracy. These errors stem from unstable lighting conditions throughout the flight and the NIR sensor malfunction. The malfunction caused the NIR bands not to be recorded, a wavelength range which was shown to be highly relevant when separating grassland communities. A first classification of the grassland classes within the orthomosaic has a low accuracy, which is in part due to botanists' class definitions, that were unsuitable for spectral classification, as well as changing light conditions and the sensor failure. Nevertheless, when inspecting the spectrometer data and the orthomosaic image bands, the grassland surrounding the blaiken was found to have a distinct species composition and a distinct spectral signature, as shown by the spectral signature evaluation and spectral separability test. A better classification for identifying grassland with higher blaiken risk was found to be obtained by using a different selection of classes. The low accuracy of that map suggested that the Rikola UAV data does not fit the requirements to classify grasslands from a botanical point of view, despite the quality limitations of the UAV data aforementioned. Thus, the grassland classes should be based on prior spectral image analysis. Better weather conditions (overcast sky) during the flight should also enhance the classification as it reduces the influence of shadow artefacts in the image. Furthermore, species richness and NDRE (Normalised Difference Red Edge Index) values were found to be potentially connected to blaiken and erosion risk.

Keywords: Physical Geography, Ecosystem Analysis, Shallow Erosion, Blaiken, UAV, Hyperspectral Imaging, Alps, Grassland, Spectral Signatures

Advisors: Abraham Mejia Aguilar, Virginia Garcia-Millan

Master degree project 30 credits in the Master's Programme of Geomatics, 2019

Department of Physical Geography and Ecosystem Science, Lund University. Student thesis series INES nr NGEM01

Contents

1	Introduction	1
2	Background	4
2.1	Grasslands and shallow erosion in the Alps	4
2.1.1	Grassland in the Alps	4
2.1.2	Blaiken	5
2.2	Reflectance and spectral signatures	6
2.3	Grassland monitoring	6
2.4	UAV Remote sensing	7
2.4.1	UAV overview	7
2.4.2	Sensor systems for UAVs	8
2.5	Remote sensing of grasslands	8
3	Materials and methods	10
3.1	Study area	10
3.1.1	Climate	11
3.2	Data Collected	13
3.2.1	Ground survey	13
3.2.1.1	Vegetation survey.	13
3.2.1.2	Spectral fieldwork setup and sample selection.	14
3.2.1.3	Rikola photos on the ground.	16
3.2.2	UAV Rikola data	17
3.2.2.1	Flight and sensor setup.	17
3.3	Methods	18
3.3.1	Spectrometer processing	18
3.3.2	Rikola ground data	18
3.3.2.1	Pre-processing	18
3.3.2.2	Separability analysis.	20
3.3.2.3	Band reduction.	21
3.3.3	UAV Rikola Data	21
3.3.3.1	Pre-processing.	21
3.3.3.2	Orthomosaic generation, accuracy and resolution.	22
3.3.3.3	Principle component analysis	26
3.3.3.4	Normalized difference red edge index	26
3.3.3.5	Separability analysis.	26
3.3.3.6	Maximum likelihood classification.	27
4	Results	29
4.1	Relationship of grassland ecology and spatial distribution	29
4.2	Spectral analysis at ground level	30
4.2.1	HR1024i spectral signatures	30
4.2.2	Rikola’s spectral signatures from ground level	30
4.2.3	Spectral separability of grassland classes in ground level Rikola images	32
4.2.4	Inter- and intra-species spectral differences	33
4.2.5	Band reduction (Rikola ground images)	34

4.3	UAV data analysis	35
4.3.1	Spectral separability of grassland classes in UAV orthomosaic . . .	35
4.3.2	Grassland communities map based on botanic classification	36
4.3.3	Grassland communities map based on spectral classes	37
5	Discussion	39
5.1	Limitations of the study and recommendations	43
5.2	Future Research	45
6	Conclusion	46
	References	47
	Appendices	51

List of Figures

1	Blaiken erosion in the North Tyrolean Alps	2
2	Blaiken types	5
3	Maps of the study area	10
4	Climatology of the study area: Schlüterhütte	12
5	Cloud coverage of the study area: Schlüterhütte	12
6	Vegetation areas and sample site distribution	13
7	Grassland sample areas	14
8	Equipment and sensor overview	15
9	Mission plan & UAV setup	18
10	UAV data processing flow chart	22
11	UAV orthomosaic extent	23
12	Sample area spectral signatures: Ground vs. UAV	25
13	Spectral signatures of sample areas	31
14	Spectral signatures of calibration targets: Reference, raw DN & calibrated	31
15	Spectral signatures of <i>Nardus stricta</i>	33
16	Effect of light conditions on leaf reflectance	34
17	Sample area band correlation	34
18	Maximum Likelihood Classification of grassland community classes	36
19	PCA orthophoto	38
20	NDRE image from orthophoto	38
21	Maximum Likelihood Classification of spectrally distinctive classes	38
A1	Maps of the study area (large)	51

List of Tables

1	Grassland communities	13
2	Rikola hyperspectral camera wavelengths	17
3	Plant survey excerpt	29
4	Separability between vegetation classes in ground Rikola images	32
5	Separability between grassland community classes in UAV Rikola images	35
6	Accuracy of MLC maps, based on vegetation classes	36
7	Accuracy of MLC maps, based on spectral classes	38
A1	Complete plant survey	52

Abbreviations

ERODYN Project studying Shallow EROsion DYNamics in mountain grasslands of South Tyrol

EURAC European Research Institute in Bolzano

GCP Ground Control Point

GPS Global Positioning System

HR1024i SVC HR1024i Field Spectroradiometer

IR Infrared spectrum (Wavelengths between 0.7 μm and 1000 μm)

JMD Jeffries-Matusita Distance - a measure for class separability

m.a.s.l. meters above sea level

NDRE Normalised Difference Red Edge Index

NDVI Normalised Difference Vegetation Index

NIR Near infrared Spectrum (Wavelengths between 0.75 μm and 1.4 μm)

PCA Principle Component Analysis

RE Red Edge infrared Spectrum (Wavelengths between 0.7 μm and 0.75 μm)

RGB Red Green and Blue

Rikola Senop Rikola Snapshot hyperspectral camera

TDSI Transformed Divergence Separability Index - a measure for class separability

UAV Unmanned Aerial Vehicle

UNIBZ University of Bolzano

UNIIB University of Innsbruck

1 Introduction

The alpine grasslands as a cultural landscape, over centuries, has maintained a balance which meets the needs of local agriculture, a florally highly diverse habitat and tourism industry, which has become an important economic factor in the region (Väre et al., 2003). Changes in the environment caused by the abandonment of agricultural land impacts the region on many levels and persists over the last 150 years (Rutherford et al., 2008). Pasture abandonment led to natural reforestation which decreases the aesthetic value by 10 % to 15 % and negatively impacts tourist revenue (Schirpke et al., 2016). The abandonment of high alpine pastures has also been linked to an increase in grassland erosion (Tasser, Mader and Tappeiner, 2003). This not only damages the aesthetics of the cultural landscape but also the floral habitat and the soil layer. Landslides in the mountains are also a hazard. Maintaining the alpine grassland landscape is therefore of interest to local government in hope to preserve traditional agriculture, the natural diversity and tourism in the Alps.

Steep slopes and harsh climate at high altitudes make soils prone to many forms of erosion, one type of which are blaiken. Blaiken are a minor and understudied form of shallow erosion. Stahr and Hartmann (2013) describe blaiken as bare soil patches with little to no vegetation and resulting from sheet-landslide events occurring on slopes of high alpine grasslands. A healthy grassland is important as it helps to maintain the unstable and limited amount of soil in the area (García-González, 2008). Studies over the recent years have shown an increase of blaiken (Blechs Schmidt, 1990; Meusburger and Alewell, 2008; Schauer, 1975; Tasser, Tappeiner and Cernusca, 2005; Wiegand and Geitner, 2010) and suggest a connection to changes in pasture and meadow management. They are believed to be triggered by nival effects in most cases. An example of this phenomenon in the Austrian Alps can be seen in Figure 1. When assessing blaiken erosion, Tasser, Mader and Tappeiner (2003) found land use as one of the most determining factors of erodibility. Their findings show that abandoned, previously managed meadows show an increase of vegetation types (mainly tussock grasses and dwarf shrubs) with less potential for soil stabilization. Instead, they increase snow gliding or transfer the downward force of the snow weight into the ground via frozen shrubs and create tension fissures in the soil. These factors have been found to increase the likelihood of blaiken erosion (Tasser, Mader and Tappeiner, 2003).

Soil conservation efforts can reduce blaiken erosion. In order to focus these efforts on the most sensitive areas, it is necessary to map relevant grassland species related to erosion. It has been shown that grassland species around blaiken differ to those areas not affected by blaiken erosion. (Tasser, Mader and Tappeiner, 2003). These differences in grassland communities are likely to display different spectral signatures which in turn



Figure 1: Blaiken erosion in the North Tyrolean Alps (photo from autumn 2017 by Andreas Mayr (ERODYN, 2018))

could be used to categorize the vegetation into "susceptible to erosion" and "less susceptible to erosion". Multispectral images have been used for vegetation monitoring in many forms but might not be sufficient for distinguishing grassland. Hyperspectral cameras are more sophisticated than multispectral cameras and promise advantages in vegetation monitoring as they can capture many more spectral bands than traditional image sensors. Lopatin et al. (2017) have demonstrated that spectral differences in grasslands are detectable, but classification is only possible for a small number of classes. By not relying on the detection of single species classes, but a mixed signal of the vegetation (grassland communities) it might be possible to achieve good separability of vegetation classes. Hyperspectral images have the potential to distinguish various grassland communities and could be indicative of certain blaiken-influencing factors, such as soil composition or soil moisture. These sensors may also be able to identify vegetation forms which directly influence the stability of the surface soils due to their root structure or the above ground plant structure. Field surveys are not well suited for producing maps of an area continuously, while satellite remote sensing mapping of vegetation (Sentinel-2) lacks the required spatial resolution, as the erosion areas manifest in extents of 2-10 m in diameter (Tasser, Mader and Tappeiner, 2003) while the map resolution of Sentinel-2 is 10 m in the best case. Classifying vegetation types using hyperspectral remote sensing data collected by Unmanned Aerial Vehicle (UAV) can potentially overcome both issues: spectral and spatial resolution.

The project on Erosion Dynamics (ERODYN) (ERODYN, 2018) conducted by the University of Innsbruck (UNIIB) in collaboration with University of Bolzano (UNIBZ) and the European Research Institute in Bolzano (EURAC), intends to develop a more

comprehensive understanding about blaiken erosion in the Alps. The role of vegetation in Alpine blaiken erosion is addressed by UNIBZ and EURAC. UNIBZ focuses on the bio-physiological properties whereas the EURAC team studies vegetation through remote sensing.

Grassland species in blaiken areas have the potential to act as an indicator for blaiken risk in the Italian Alps. This work aims to evaluate the capabilities and limitations of the innovative Rikola hyperspectral camera mounted to an UAV in the context of vegetation monitoring related to blaiken areas. It was carried out in a typical blaiken afflicted site near the Schlüterhütte with data collected during a field campaign in July 2018. The main objective is to answer the question:

Do UAV-based orthomosaics from images of the Rikola Snapshot hyperspectral camera have the potential to accurately capture spectral signatures of the grassland communities related to blaiken areas?

Secondary goals are the following:

- To verify the accuracy of the Rikola hyperspectral camera using the SVC HR1024i field spectroradiometer.
- To evaluate the grassland composition around the blaiken erosion patches, identifying patterns and relevant species.
- To determine the spectral separability of vegetation classes within Rikola hyperspectral images taken on the ground and from UAV.
- To create a classification map of vegetation types in the vicinity of blaiken erosion areas using orthophotos created from Rikola hyperspectral images.

2 Background

This chapter examines previous research and knowledge on the topics touched on by this thesis. It begins with an introduction about the studied grassland environment and research on shallow erosion (blaiken erosion) processes in the Alps. Then follows a section which explains how this spectral information can be used for grassland monitoring. It concludes with details about UAV mounted sensors used during this research, UAV specific sensors and the intricacies about processing that data.

2.1 Grasslands and shallow erosion in the Alps

2.1.1 Grassland in the Alps

Grasslands are a highly diverse group of vegetation and one of the most widespread ecosystem on the planet, growing in almost all climate zones from tropical to temperate and associated with many soil types. They can be considered a transitional vegetation zone between areas with unsuitable (desert) and extremely favourable growth conditions (forests). One of the main reasons for their distribution is, to a large extent, the human-driven expansion of pastures and food crops. Grass has a fast growth rate and high recovery potential, especially after disturbances such as fire, grazing and mowing. In conditions with regular disturbances grasslands vegetation therefore has a natural advantage over other woody and taller vegetation types such as forest or shrubs (Encyclopædia Britannica, 2018). While the species diversity within natural and semi-natural grasslands is quite limited, the overall native biodiversity of grasslands between different habitats is high. This is due to the adaptation of the plants to the wide range of locations and vegetation limiting factors (Risser, 1988, p.176).

On the Eurasian continent, the European Alps are considered to be a hot-spot in terms of vegetation diversity. The range of habitats is diverse because of big changes in altitude, topography and soil types resulting from the many rock types present in the Alps (Leuschner and Ellenberg, 2017, p.271). Alpine grasslands and herb communities appear in montane and subalpine areas mainly because of natural disturbances such as avalanches or human deforestation for agricultural purposes. Widespread natural grassland areas establish above the dwarf shrub biome and the individual tree line, approximately from the middle alpine to the sub-nival altitudinal zone (Leuschner and Ellenberg, 2017, p.289).

Of particular interest to this study is the grassland's function and potential for soil stabilisation and erosion prevention because of the grasses' fine, dense root structure as outlined by Reubens et al. (2007). The importance of vegetation with high root density and length is also pointed out by Tasser, Mader and Tappeiner (2003) for its role in blaiken erosion mitigation.

2.1.2 Blaiken

Blaiken have become an increasing problem within alpine grasslands. The main processes involved in blaiken erosion are a combination of snow gliding and under-wash of soil with a structural sliding disposition because of a sudden change in soil layers (Blechsmidt, 1996). Blaiken types are differentiated by their genesis. 1. *Schneeschorfblaiken* (snow scraping blaiken) appear due to slow layer-by-layer scraping of the soil by gliding snow. 2. *Schneedruckblaiken* (snow pressure blaiken) result from downslope movement of heavy snow masses being blocked by obstacles such as sturdy shrubs which transfer the pressure of the snow weight into the soil via the root system and finally cause the whole vegetation-soil-mass to slide downhill (Zweckl and Spandau, 1987). Small, slope parallel, tension fissures, usually caused by snow creeping, are the initial stadium of 3. *Blattanbruchblaiken* (soil fissure blaiken). These occur in springtime when snowmelt water penetrates the fissures, undermining the soil stability. The three different types of erosion are illustrated in Figure 2.

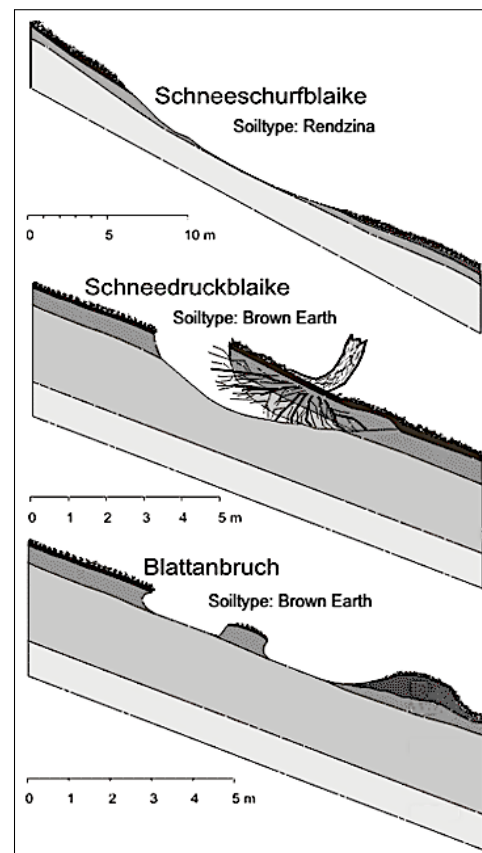


Figure 2: Blaiken types (modified after Stahr, 2014)

Tasser, Mader and Tappeiner (2003) studied factors contributing to blaiken erosion in the Alps to determine the contribution of land use and land use change. Of the twelve statistically significant factors they studied, land use was shown to have a significant impact on erosion probability. 72% of landslides occurred on abandoned pastures against only 25% in actively managed ones. The study also investigated the difference in vegetation composition and its influence on snow glide. It found that certain plants such as tall dwarf shrubs, tree saplings and *Rhododendron ferrugineum* are present in low erosion risks areas, while species expected to show in high-risk areas are dwarf shrubs such as *Arctostaphylos uva-ursi*, *Calluna vulgaris*, *graminoids* and tussock grasses (Tasser, Mader and Tappeiner, 2003). Their study confirmed the erosion risk correlation of *Alnetum viridis*, dwarf shrub- and grass-coverage as well as root length and density and showed that herb coverage has no significant correlation. Other highly significant factors were confirmed to be exposition, slope, management level and soil depth.

Blaiken erosion is an understudied phenomenon which requires much research in many

directions to eventually form a solid understanding of all of its elements. However, blaiken erosion seems to be more likely in areas with abandoned pastures due to the resulting vegetation. Therefore this type of grassland vegetation might be a good indicator for future blaiken areas.

2.2 Reflectance and spectral signatures

The aim of this thesis is to test if images from an UAV mounted hyperspectral camera can be used to distinguish different types of grassland vegetation in the vicinity of blaiken. Hyperspectral imaging devices record the light reflected into the sensor over a range of the electromagnetic spectrum from a large number of very narrow bands, virtually creating a continuous spectral dataset. This information allows to calculate a detailed and accurate spectral signature for every pixel in the image. The usefulness of capturing reflectance is based on the assumption that each material has a unique spectral signature that can be used to identify different materials using the appropriate sensor (Cochrane, 2000).

To understand what a spectral signature is, one first needs to understand the concept of reflectance, as a spectral signature is comprised of a quasi-continuous measurement of reflectance within a specified wavelength spectrum. When incoming light hits an object such as a plant leaf, some of the energy is absorbed by the leaf while the rest is reflected or transmitted. This ratio between the reflected light to the amount of incoming light is a unitless percentage known as reflectance (R) (Jensen, 2015). Reflectance of a material varies over the electromagnetic spectrum depending on its structure and composition, such as leaf thickness and water content and also depends on the position of the source of light, the observed object and the position of the sensor with respect to each other. A spectral signature is the curve representing the variation in reflectance of a material over a continuous electromagnetic spectrum. When recorded in high detail and accuracy, it is presumed to be a unique identifier for vegetation species or communities (Price, 1994).

2.3 Grassland monitoring

Identifying vegetation can be approached either by ground data collection or remote sensing. Ground surveying and *in situ* measuring devices have the potential to be very accurate and precise. They often consist of vegetation identification by visual inspection by experts. Spectral measurements by multispectral cameras or spectrometers, have also been used to analyse vegetation (Ali et al., 2016). With spectral information, experts classify the vegetation by categories including biological family, functional types, biomass and many others. Compared to remote sensing approaches, surveying and spectral measurements on the ground collect high quality data at individual points and at local small-scale areas. However, ground measurements are inherently ineffective for collecting

continuous data over larger areas. Continuous measurements covering large areas are, in most cases, only feasible via a remote sensing approach. Spectral cameras and sensors provide valuable information for grassland monitoring on a large spatial and/or temporal scale.

A typical spectral signature of grassland vegetation (between 400 nm and 900 nm in peak growing season) has low values in the visible spectrum with a small peak in the green spectrum, steep rising reflectance in the red edge spectrum and strong, flat reflectance in the IR wavelengths. The characteristic slopes between green, red and blue and between red and NIR are commonly used to calculate spectral vegetation indices (SVI). It has been largely demonstrated that SVIs relate to certain vegetation conditions such as chlorophyll content, water content or biomass and could therefore be useful for differentiating types of vegetation, including grasslands. The best known Normalised Difference Vegetation Index (NDVI) is calculated from wavelengths red (680 nm) and infrared (IR) (800 nm) and shows a strong correlation to chlorophyll content and vegetation biomass (Tucker, 1979). The wavelength bandwidth of red edge (700 nm – 750 nm) is a good estimator of chlorophyll content and, by extension, vegetation stress and is used in the Normalised Difference Red Edge Index (NDRE) (Dawson and Curran, 1998; Pinar and Curran, 1996).

2.4 UAV Remote sensing

Remote sensing technologies have been used for decades and are conducted from satellites, aerial imagery and UAVs. When it comes to obtaining remote images for non-destructive surface analysis, UAVs have rapidly grasped the interest of researchers worldwide due to their relative affordability, rapid repeatability, high ground resolution as well as site-specific application, height and sensor adaptability. Classes of UAVs usually used are: (helium) balloons, fixed wings, gliders and quatro-/hexa-/octocopters (Themistocleous, 2014).

2.4.1 UAV overview

The most versatile, and also the vehicle used in this study, is the octocopter. An octocopter platform usually consists of the following: flying platform, onboard computer, GPS module, gimble, the sensor system and possibly an irradiance sensor for sensor calibration (Cruzan et al., 2016; Ishida et al., 2018). As most multi-copter drones, it can take off and land from small flat areas, it is highly controllable in the air and stable during the flight, due to a gyroscope, self-stabilizing software and a mechanical stabilization gimbal for sensors. It can be programmed to fly a pre-programmed flight path using the Global Positioning Service (GPS) for optimized ground coverage and overlap. Because it has

more propellers and has a larger size, the octocopter is superior to other drones due to its increased flight stability and payload capacity. In many situations the octocopter is, therefore, a superior tool for remote sensing compared to the other UAV alternatives.

Disadvantages of UAVs in general are the relatively high cost, the requirement of a dedicated and trained pilot, the need for flight permission and low operation time of about 20 minutes per flight due to battery limitations. UAV field studies require elaborate field trips to locations. Wind, clouds and weather can interfere with data collection and data quality. Multispectral or hyperspectral sensors require stable flight and light conditions because they usually feature slower sensor speeds and collect data over an extended period of time (Chang and Clay, 2016).

2.4.2 Sensor systems for UAVs

A typical assortment of UAV optical imaging systems for vegetation monitoring are: consumer RGB cameras, converted consumer IR cameras, thermal imaging cameras, multi spectral cameras and spectrometers (Von Bueren et al., 2015; Berni et al., 2009). A more recent addition are lightweight and compact hyperspectral cameras. These cameras have, through miniaturisation, been available for UAV systems since 2013 and fill the niche for spectral information at a high temporal and pixel resolution. Compact hyperspectral cameras have been of particular interest to the agricultural sector, where they show promising results for crop monitoring, nitrogen content measurements, biomass measurements, crop yield and crop stress (Bareth et al., 2015). The Rikola hyperspectral camera used in this research houses two sensors of the "Fabry Perot" type, which utilises a system that allows only specific wavelengths to pass a thin air gap between two mirrors. By being able to precisely change the gap distance between the mirrors, this creates a tunable optical filter which allows the instrument to measure one wavelength at a time (Senop Optronics, 2014; Saari et al., 2009).

2.5 Remote sensing of grasslands

To detect and classify grassland vegetation types, a remote sensing approach is the simplest. It is also much better suited to transfer the results of the study to other blaiken sites. Recent studies by Wiegand and Geitner (2010) and Wiegand and Geitner (2013) have also suggested a remote sensing approach to gain further insight into these erosion dynamics both for monitoring the vegetation and changes to the erosion extent.

Vegetation classification. Classifications summarize vegetation by splitting it into groups with similar properties. Many supervised and unsupervised classifications techniques exist to separate, visualise and quantify differences in vegetation. It has been

proven that classification maps are most effective in separating vegetation and non-organic surfaces, but they can also distinguish different vegetation types and classify many parameters of vegetation such as biomass and vitality (Prasad S. Thenkabail, 2016, p.12).

Classification of vegetation can be done with indices, such as the NDVI, by applying threshold values that separate vegetation from other classes or different vegetation. However, classification algorithms are a more commonly used classification technique. While classification algorithms are not specialised for a specific land cover, they develop custom classification rules from the datasets. Supervised classifiers require training data (i.e. Maximum Likelihood, Object-Based, Support Vector Machine), while others work unsupervised. Despite the existence of a multitude of vegetation monitoring indices and classification techniques, studies classifying individual species in grasslands using hyperspectral data, have demonstrated how challenging this can be (Lopatin et al., 2017; Möckel et al., 2016). Because of the similarities of spectral signatures between species, classifications showed low accuracy. The spectral signature of a group of plants might be distinct enough from another group adapted to different environmental conditions in order to achieve successful spectral class separation. Recent research such as that conducted by Brenner, Christman and Rogan (2012) points out that when classifying grasslands, which have very similar spectral properties and high within-class variability, improved results can be obtained from a maximum likelihood classification in combination with object-based segmentation due to its incorporation of spatial information.

Separability estimators such as the Jeffries-Matusita Distance (JMD) and the Transformed Divergence Separability Index (TDSI) are both methods which measure the statistical separation between the classes of the chosen training areas and thereby indicate their potential to be classified and distinguished from one another. These estimators help to determine the most useful bands for maximum likelihood classifications.

3 Materials and methods

This study investigates the use of UAV based hyperspectral imaging for grassland monitoring in the context of blaiken erosion. The following section will first elaborate on general information about the flight campaign, the fieldwork setup and sample area selection. It then elaborates on ground sampling and ground measurements of the grassland's spectral properties. An upscaled version of the hyperspectral ground measurements was recorded from the air with the same camera mounted UAV. The ground data was used to evaluate and verify the hyperspectral orthomosaic which was created from the aerial images.

3.1 Study area

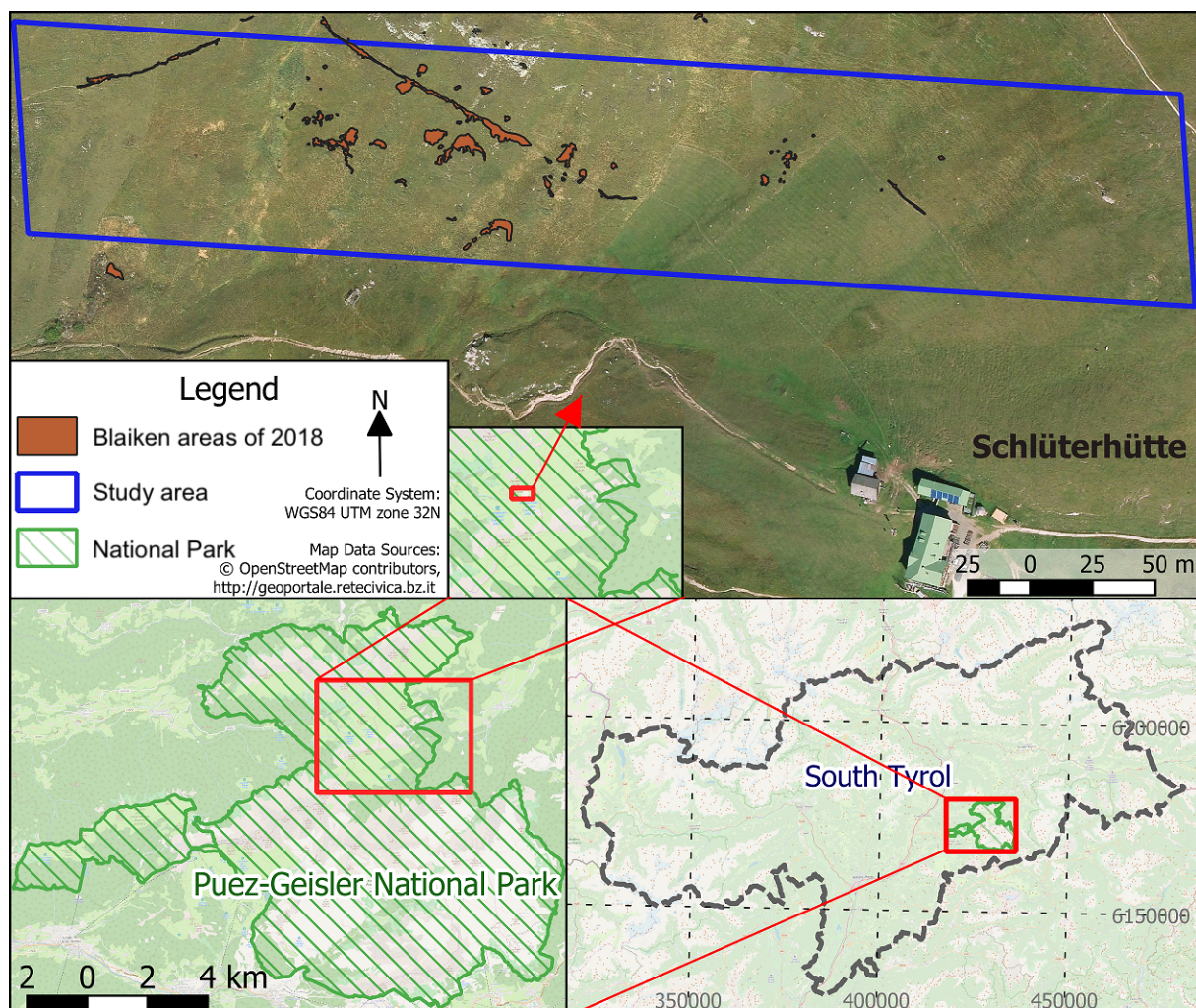


Figure 3: Maps of the study area – The map shows the location of the study area in the state of South Tyrol, Italy. The main image displays the grassland area near the Schlüterhütte and illustrates the blaiken erosion areas as they existed in June 2018 (full size map in the appendix, Figure A1)

The study area is located near the Schlüter alpine lodge (2306 m.a.s.l.) which lies within the Dolomite mountain range of the Italian Alps in the Puez-Geisler Nature Park, about 30 km northeast of South Tyrol's state capital of Bolzano (Figure 3). The relief of this region stands out due to its immense changes in altitude with high peaks, the highest being the *Sass Rigais* at 3025 m.a.s.l., and wide, deep glacial-period valleys. The sedimentary rock of these formations is mainly composed of carbonate rock dolomite, which builds out sharp peaks and large debris areas with sparse vegetation due to karstification (dissolution of soluble rocks) and congelifraction (cracking and destruction of rocks by expanding, freezing water in rock cracks). In areas where these processes have subsided, the more gentle topography allows for fertile pastures and grass dwarf-shrub heaths above the tree line (Autonome Provinz Bozen-Südtirol, 2011).

It is an area historically used for cattle grazing, where a large area has been abandoned due to economic factors and erosion damage. Other human activity in the area is tourism. Hiking trails exist below the blaiken areas and on the mountain ridge above. Some less frequented trails run within the erosion area. Many areas of blaiken erosion can be found west of the Schlüter lodge on a south-west facing slope of the valley. These partly managed grasslands are the focus of this study. While the area closest to the lodge shows clear signs of recent management such as mowing, the rest of the area has reverted to a more unmanaged state (see Figure 3). An eroded path running east to west traverses the area a couple of meters below an exposed rock cliff. Most erosion areas lie just below this path and cover between 0.1 m and a maximum of 10 m in diameter. Two types of erosion can be identified: 1. Long eroded areas along and around the footpaths, which also show occasional downhill outcrop areas. 2. Small and large, roundish bare soil areas within the grasslands. Which of the three blaiken causes are responsible for the erosion is difficult to ascertain without further study such as soil analysis, but some blaiken areas show sharp edges. This and the lack of apparent shrubs indicate the main trigger might be tension fissures (the cause of soil fissure blaiken). There are some convex areas of sparse grass where the bedrock penetrates the surface within the pasture and surrounding the cliff areas above, while about three concave strips, presumably water drainage areas, of more lush grassland communities formed, traversing the meadow down-slope.

3.1.1 Climate

Figure 4 describes the climate of the area. The monthly average temperature ranges from -10°C in February to $+10^{\circ}\text{C}$ in August. Annual precipitation is 630 mm, with the most precipitation occurring in June. This places it firmly in alpine tundra climate (*ET* of the Köppen climate classification).

Working with remote sensing data and UAVs requires special attention to wind speed

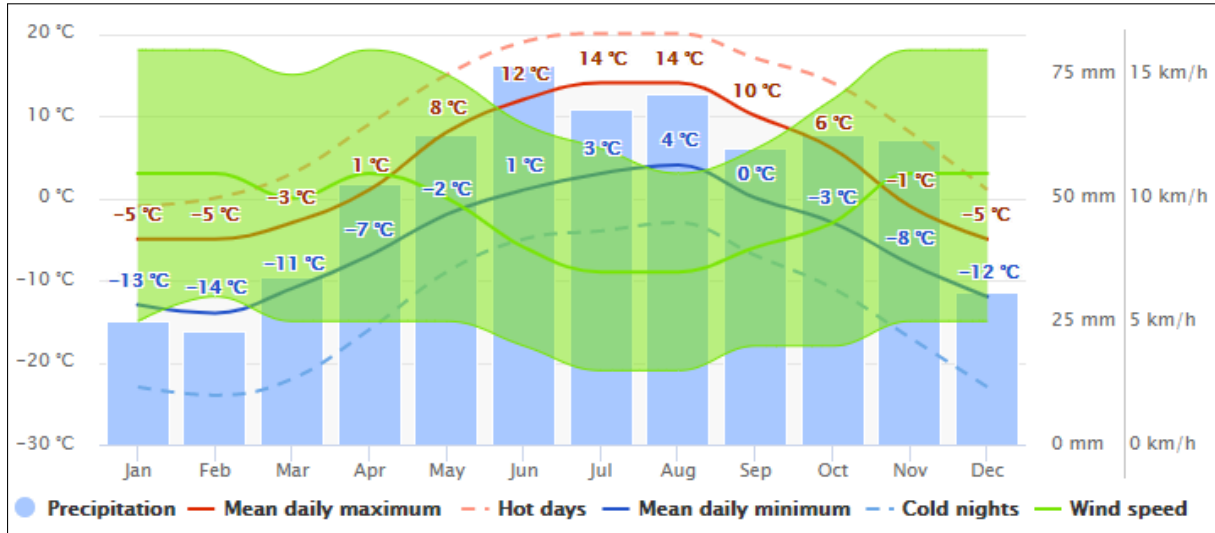


Figure 4: Climatology of the study area: Schlüterhütte, South Tyrol, Italy, 630mm, 1.5°C, (46.64°N 11.8°E 2306m), source: meteoblue (2018)

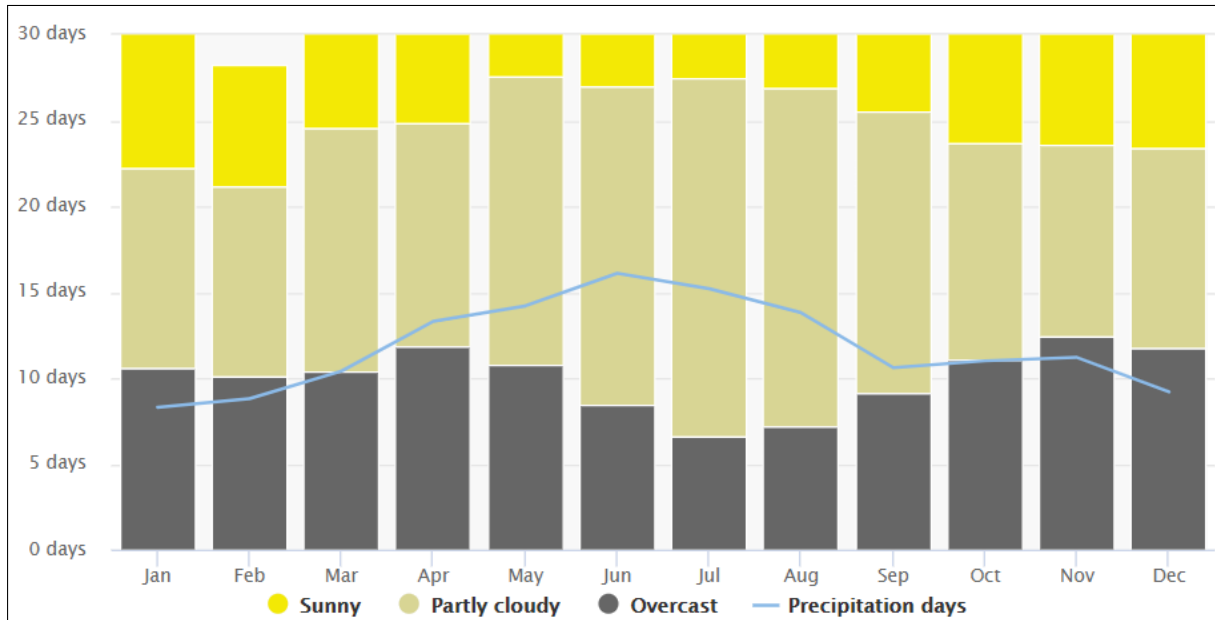


Figure 5: Cloud coverage of the study area: Schlüterhütte – (46.64°N 11.8°E 2306m) source: meteoblue (2018)

and cloud cover. Low wind speeds and uniform cloud conditions, such as completely overcast or clear sky are required for flight safety, long flight times and data quality. Figure 4 shows the average wind speed in the area fluctuating between 5 and 15 km/h (1.4 - 4.2 m/s) with lowest speeds during the summer months of July to September. The same period also coincides with the period of the highest chance for a partly cloudy sky (Figure 5). The chance for completely overcast or cloud-free days is only between 9 and 13 days per month in the summer while the highest chance for good cloud conditions is from November to February.

3.2 Data Collected

3.2.1 Ground survey

3.2.1.1 Vegetation survey. UNIBZ conducted a plant survey of the species ground cover % in each sample area. The data was organised and analysed in order to find grassland vegetation patterns within or between sample areas and to detect key species of blaiken grassland. The survey was performed by Ecology PhD students from UNIBZ, who determined continuous areas with homogeneous grassland cover types shown in Table 1. They visually identified and quantified the shares of vegetation cover within the sample areas (Figure 6 and Figure 7).

Table 1: Grassland communities – The 8 classes identified and mapped by the Ecologists of UNIBZ

Class	Short description	Dominant species and % coverage				Bare soil % coverage	No of Species	
		1st dominant	2n dominant	3rd dominant				
A	Abandoned pasture	<i>Nardus stricta</i>	20-33	<i>Arnica montana</i>	12.5-20	7.5-20	10 ; 7	
B	Natural pasture	<i>Nardus stricta</i>	33	<i>Leondonton helveticus</i>	20	0	9	
C	Dry grassland	<i>Poa spp</i>	50	<i>Nardus stricta</i>	33	0	11	
D	Blaiken (little erosion)	<i>Geranium sylvaticum</i>	12.5-50	<i>Festuca spp</i>	4-50	<i>Alquemilla ssp</i> 0-33	0	5 ; 7
E	Blaiken (strong erosion)	<i>Horminum pyrenaicum</i>	0-50	<i>Festuca spp</i>	0-33	<i>Bromus spp</i> 0-33	0	7 ; 7
F	Humid grassland	<i>Alquemilla spp</i>	33	<i>Nardus stricta</i>	20	<i>Selseria varia</i> 20	0	6
G	Pasture	<i>Leondonton helveticus</i>	30	<i>Selseria varia</i>	20	0	9	
H	Mowed pasture	<i>Nardus stricta</i>	20-33	<i>Potentilla erecta</i>	7.5-12.5	0	13 ; 3	

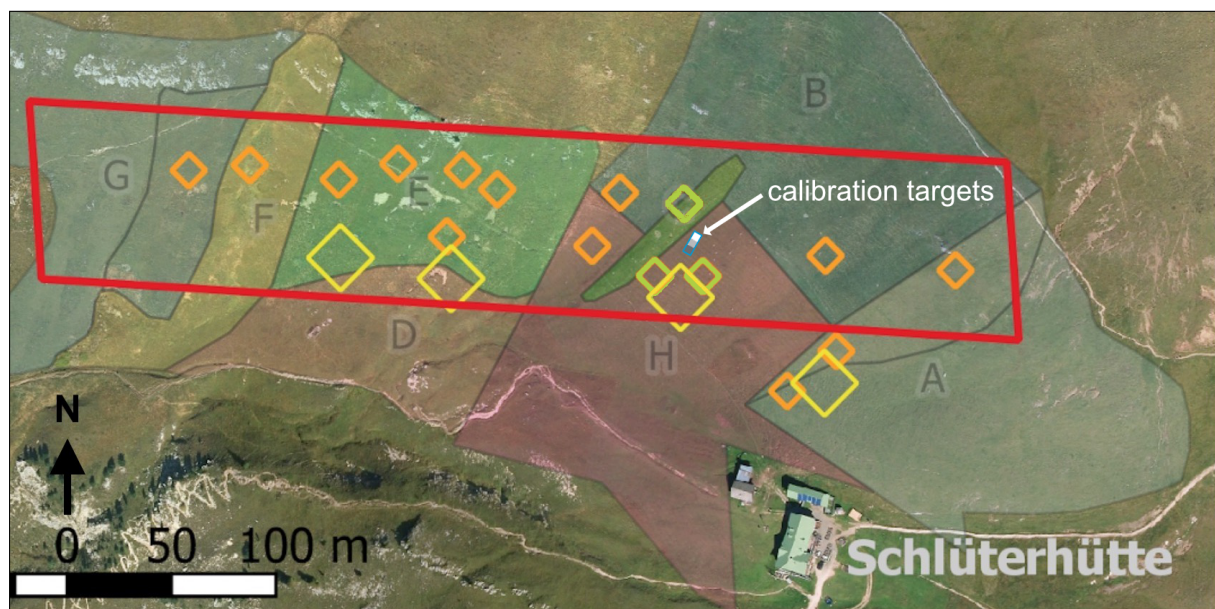


Figure 6: Vegetation areas and sample site distribution – Grassland communities are labeled A to H (Table 1), the intended area of interest is framed in red. The sample areas of 30 cm² and 5 m² are indicated by small orange (and 3 green) and large yellow squares respectively. (central coordinates: 46°38'10.3"N 11°48'13.0"E)

Additionally, three sample areas of 5 m^2 within the most dominant areas were surveyed, in order to achieve a more representative vegetation assessment. This vegetation survey provided the classes for the grassland communities' map generated from hyperspectral UAV data.

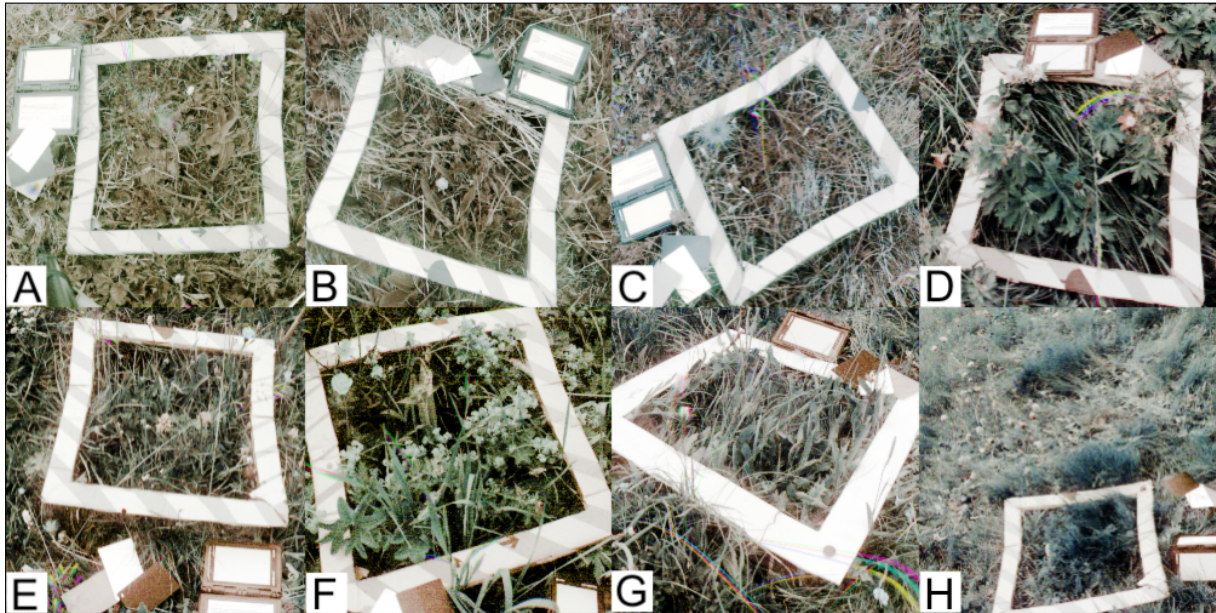


Figure 7: Grassland sample areas – Rikola hyperspectral images (ground recordings) from all eight grassland classes (Table 1)

3.2.1.2 Spectral fieldwork setup and sample selection. The main goal of this study was to evaluate the quality of the Rikola hyperspectral UAV data. Recent and high-resolution hyperspectral data of the blaiken erosion area was obtained during a field campaign in order to cross-validate the accuracy of the UAV sensor data. Two kind of measurements were done on the ground to assess the accuracy of the UAV images: (1) High quality spectral signatures recorded with the SVC HR1024i field radiospectrometer (Spectra Vista Corporation, Poughkeepsie, USA) (HR1024i) and (2) Rikola hyperspectral photos over the grassland. The measurements coincided with the samples of grassland for the botanic survey, which are meant to be the classes of the resulting map that will be generated with the UAV orthomosaic. The Rikola photos on the ground were meant to control for effects caused by the camera being mounted on a UAV. High precision GPS coordinates were recorded for precise sample area location and georeferencing. As briefly mentioned before, a vegetation survey of the sample areas was also conducted to assess vegetation patterns from an ecological point of view. An overview of the equipment and sensors used in this research can be found in Figure 8.

The campaign was conducted on 10th and 12th of July 2018 between 10.00 am and 06.00 pm. This date was chosen to coincide with the peak phenology period of the alpine

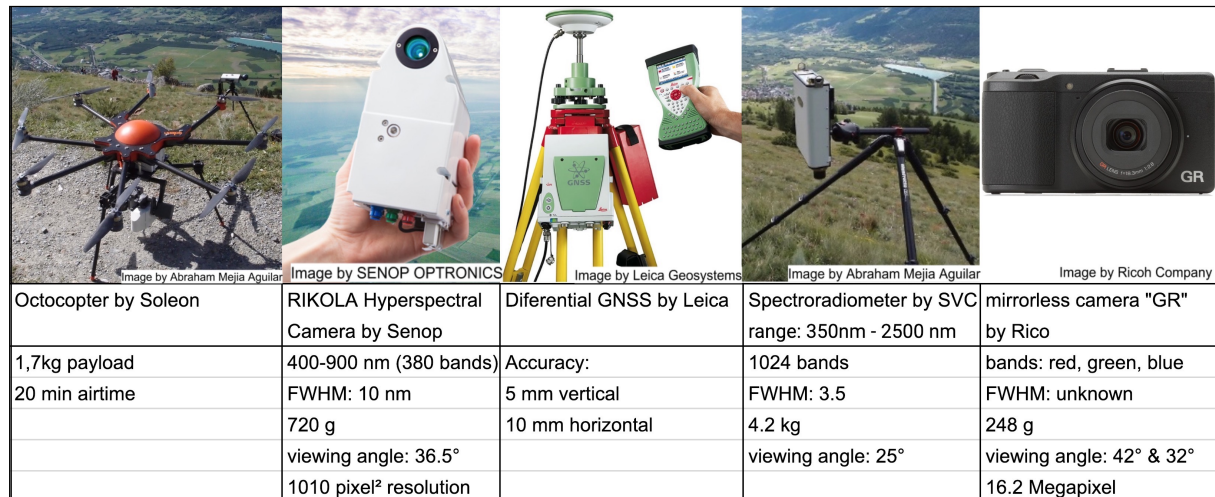


Figure 8: Equipment and sensor overview – Overview about the technical equipment used during the field campaign at Schluter Hütte

grasslands. Peak vegetation period occurs in July/August in the Swiss alpine grasslands (Fontana et al., 2008). The vegetation was moist in the morning and dried during the day. The weather was dry overall until oncoming rain towards the end of the second day. The field work was conducted within a collaborative project, comprised of a team from UNIIB, UNIBZ, as well as Abraham Mejia Aguilar and the author, who were working for EURAC, all gathering data for the ERODYN Project (ERODYN, 2018). Colleagues from the Applied Botany Institute of UNIBZ accompanied the field trip as experts to create a preliminary map (Figure 6) of different grassland areas and perform the vegetation survey.

Three sampling points were chosen randomly within each of the eight land cover type areas shown in Figure 6. However, types B (natural pasture), C (dry grassland), F (humid grassland) and G (pasture) were only sampled once; B because of its similar vegetation to A; C due to it being a relatively small area; and the remaining samples of F and G had to be forgone due to approaching rain weather and in order to be able to record three samples of the vegetation type H, which was of more importance, due to it being a managed pasture which had been deemed highly relevant for mitigation of blaiken risk by Tasser, Mader and Tappeiner (2003). For this survey we used a map that was a preliminary, generalized representation of the actual vegetation; therefore, orientation in the field was difficult. This is the reason why some sample areas, which were identified as a certain grassland community, are actually found outside of their respective vegetation area on the preliminary vegetation map (Figure 6).

Images of each sample area are shown in Figure 7. Squares of 30 cm^2 were placed over the chosen sampling points and fixated to marked the sample areas. The size was chosen to be small enough to be captured by the ground-based Rikola camera and large enough to allow to be seen and sampled in the UAV Rikola orthomosaic. The orthomosaic has an

expected resolution of 3 cm/pixel at 50m flight height and an expected location accuracy of less than 3 cm, since a high precision GPS system by Leyca was used to measure the coordinates. The GPS measurements on the ground were off-set by 60 cm to the west of the sample centres, to not to disturb the vegetation that was going to be measured by the HR1024i and Rikola.

Ground control points for georeferencing. Five GCPs (Ground Control Points) were distributed throughout the area of interest and their coordinates were measured with the Leica GPS (see Figure 8). The GPCs were 50 cm in size, cross shaped and made of press-board material, which is well visible in the UAV images. GCPs are required for georeferencing and precision assessment of the orthomosaics.

Spectroradiometer measurements. The HR1024i integration time was set to 3 seconds. The height was chosen at 65 cm to achieve a 15 cm radius field of view. The HR1024i was calibrated with a spectralon disc. The disc consists of spectralon material (Labsphere, 2019) that reflects according to Lambert’s Law and has optimal reflectance values of 98 % over all wavelengths relevant for this study (500 – 900 nm). The calibration measurement is used to obtain a reference value of solar irradiance for the instrument to calculate the reflectance values of recordings over the target of interest. Each site was measured three times and averaged, following a preliminary calibration measurement of the spectralon.

3.2.1.3 Rikola photos on the ground. At each location, the Rikola camera was positioned on a tripod with its viewing angle covering the sample area square and the calibration target cards for radiometric calibration. Optimal top-down images with vertical view were attempted as much as possible but not possible due to shadow created by the tripod and the instrument. Additionally, the uneven terrain and steep slope made it difficult to achieve a stable and consistent viewing angle which produced differences in the viewing angle of the images. The integration time is set automatically by the software of the SVC HR-1024i (Spectra Vista Corp., 2012) to capture the optimal illumination in order to not over- or under-saturate the sensor. Later each image was standardised by radiometric correction using the calibration targets to remove differences due to integration time. The band setup was distributed over the whole spectrum of the camera (500 nm - 900 nm) and the final Rikola setup was configured with 27 bands of 10 nm bandwidth and the central wavelength of the bands being approximately 15 nm apart. The final wavelengths are shown in Table 2.

3.2.2 UAV Rikola data

3.2.2.1 Flight and sensor setup. The UAV that was used for the aerial data capture was an octocopter by Soleon (SOLEON GMBH, Varna, Italy), with a load capacity of 1.7 kg. Flight time, when fully equipped and including two 10,000 mAh batteries, was 20 minutes, giving it about 15 minutes for safe data collection. The flight path of each flight was 50 m long and 20 m wide with an approximate 60 % image overlap at a minimum flight height of 50 m. Due to the slow exposure time of the Rikola sensor, flight speed was set to a relatively slow rate of 1.5 m/s. The flight plan was designed with the software Mikrokopter (HiSystems GmbH, Moormerland, Germany) and uploaded to the UAV before the flight. The onboard GPS for navigation has an accuracy of 1–3 m and provided rough location estimates for each image, in order to increase processing speed for image stitching afterwards.

In order to cover the 5 hectares area of interest, the calculated flight plan required two separate and overlapping flights, due to the limited flight time. Weather conditions showed a moderate wind speed and a sky with a fast-moving patchy cloud cover.

The flights were done between 12.00 pm and 02.00 pm. They were conducted at an altitude of only 3 m due to a starting position on a ridge above the site. This was required to ensure a safe flight by keeping continuous visual contact with the octocopter and the surrounding area. This was especially important due to the irregular terrain and the possibility of hikers in the area. The start/landing point was at 2377 m.a.s.l. with the flight path taking the UAV over heights between 2352 and 2221 m.a.s.l. Flight heights above the area of interest were between 25 m and 156 m. The flight parameter and path calculations were performed by Abraham Mejia Aguilar.

The sensors mounted to the UAV were a GPS module, a high resolution mirror-less RGB camera (Ricoh GR, 16MP, CMOS-sensor, 1 img/2 sec) collecting support data for the georeferencing, and the hyperspectral imaging instrument Rikola VIS-VNIR Snapshot by Senop, with a field of view of 36.5° and 1010 by 1010 pixel image size. The Rikola

Table 2: Rikola hyperspectral camera wavelengths – The 27 chosen bands of the Rikola camera. Wav states the band wavelength in nm and FWHM (Full Width at Half Maximum) states the bandwidth of the wavelength in nm. Asterix(*) indicates the UAV Rikola image bands used for further processing while bands with two Two Asterix(**) would also have been chosen but were not available for the orthomosaic due to a sensor malfunction of the Rikola camera.

Wav	503.4*	518.2*	533.3	548.4	563.2*	578.0	593.5	608.5	622.9*
FWHM	20.2	14.6	14.2	13.8	13.5	13.2	12.9	16.7	16.4
Wav	638.2*	657.1	668.4	682.9*	698.2	712.9*	728.2**	742.9**	758.3
FWHM	16.1	16.3	16.2	16.0	15.8	15.6	15.4	15.2	15.1
Wav	773.1	787.9	803.4	818.2	833.2	848.1	863.2	878.2	893.4**
FWHM	14.9	14.7	14.6	14.5	21.7	21.5	21.3	21.0	20.8

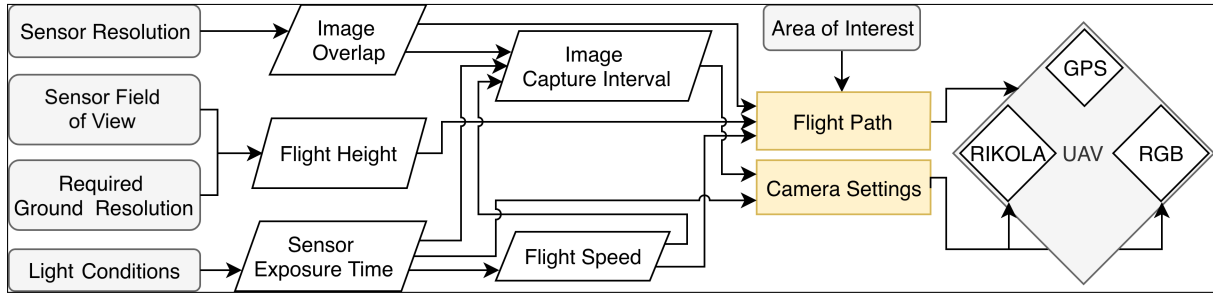


Figure 9: Mission plan & UAV setup – Flow chart explaining the camera setup and flight setup parameters

sensor was mounted on to the UAV via a three-axis gimbal. The image exposure time was set to the recommended (Senop Optronics, 2014): 15 ms for light conditions on a slightly cloudy day. The image triggering interval was set to 3 s. The Rikola setup for the flight was configured with all 27 bands shown in Table 2. A scheme showing how the sensor’s and UAV’s parameters were chosen is illustrated in Figure 9.

3.3 Methods

3.3.1 Spectrometer processing

The HR1024i spectral signature data is created in a proprietary *.sig format and requires reformatting to a *.txt in order to be readable by ENVI software (Harris Geospatial Solutions Inc., Boulder, Colorado, USA). To this end, the author developed an R script to automatically read the HR1024i files and save the data to an ENVI ASCII file. The HR1024i measures in proximately 1 nm intervals but not always exactly at full 1 nm steps. The script therefore performed spline interpolation over all measurements using the "splinefun" function of the *stats* package (*splinefun function* | *R Documentation* 2018). The interpolated signature-function was then sampled at 1 nm intervals to create a standardised spectral signature with virtual measurements at full 1 nm steps. This was done in order to standardize the output and make it compatible with the Rikola signatures when processing both together within ENVI, which could in some cases only compare and process measurements with identical sample wavelengths.

3.3.2 Rikola ground data

3.3.2.1 Pre-processing

Conversion of format. The hyperspectral images from the Rikola camera are proprietary files and required the "Hyperspectral Imager software" by the camera manufacturer (Senop Optronics, 2014) to be imported. The Rikola images were recorded as digital numbers (DN). The manufacturer provides an algorithm to convert DN into a physical

unit. In the case of this imaging sensor, the measured unit is the amount of photons at each measured electromagnetic wavelength.

The images were calibrated by subtracting a dark image taken before each measurement. The black current calibration sets the pixels that do not receive any photon to a value of zero. This sets the value of each pixel to an absolute DN. Geometric correction was performed to eliminate influences of the camera's internal components, such as lens image distortion, particularly towards the edge of the image (Senop Optronics, 2014).

As the Rikola camera is a "Fabry Perot" type, the working mechanics causes a time delay between the image capture of each wavelength. The delay can cause each band of the image to shift slightly if the camera is moving. The effect is corrected by a process called co-registration, which uses image feature detection to align the bands of each image stack. These stacks are then exported as *.tiff files (Senop Optronics, 2014).

Radiometric correction. The absolute values of the raw images are not very useful when comparing data, as the incoming lighting conditions or the sensor sensitivity are subject to changes. Reflectance (R) gives the fraction of the incoming light that is reflected into the sensor, creating comparable data. Each band of the Rikola camera requires individual radiometric correction in order to obtain images with unit-less and comparable reflectance values (Equation 1):

$$R = E_r/E_i, \quad (1)$$

where R is Reflectance in % , E_r is the light energy reflected into the sensor and E_i the incoming energy coming from the light source (e.g. incoming sunlight). It is calculated by dividing each pixel's wavelength specific E_r by E_i . The incoming sunlight was calculated by empirical line calibration to estimate the reflectance without measuring E_i or E_r (Honkavaara and Khoramshahi, 2018) (Equation 2):

$$m_\lambda = \frac{R_{t_\lambda} - R_0}{DN_{t_\lambda} - DN_{R_0}}, \quad (2)$$

where m is the slope of the linear relation between a pixel's reflectance R_{t_λ} and the measured digital number DN_{t_λ} for a wavelength. DN_{R_0} is the value at 0% reflectance (R_0).

A least two DN/R value pairs are required to find the slope m of the linear equation for each wavelength. These equations allow any R value to be calculated from a corresponding DN . The first value pair is set to a DN_{R_0} value of 0 at 0 % reflectance (R_0) by subtracting the DN values of a dark image (taken with a lens cap and with a presumed 0 % R) from the values of the original image. The second value pair requires a calibration target on the ground. Ideally, the target should be a perfect diffuse reflector that reflects light directly proportionally to the cosine of the incident angle (Lambertian surface) (Simon, 1974). In this fieldwork, the diffused reflectors were signature calibration cards with approximately

0 %, 20 %, 60% and 90 % reflectance. The 60% reflectance values R_{t_λ} over all relevant wavelengths were measured by the HR1024i and then used to calculate the linear equation for the empirical line calibration, which gives the slope m_λ for each wavelength.

Then it is possible to calculate every R_{pix_λ} (reflectance of each pixel for a specific wavelength) (G. M. Smith and Milton, 1999). To calculate R_{pix_λ} for all images and wavelengths, the author developed a batch script in the *R* language which finds the maximum values within each calibration target and sets it as DN_{t_λ} while R_{t_λ} is the known reflectance of the calibration target measured in ideal conditions with the HR1024i field spectrometer and a clamp adapter. This adapter provides a sealed measurement chamber and an artificial wide spectrum light source. The black current calibration sets $R_0 = DN_0 = 0$ and allows to calculate the reflectance of each pixel as follows (Equation 3):

$$R_{pix_\lambda} = DN_{pix_\lambda} * m_\lambda \quad (3)$$

The script not only extracts the statistical values of the sample area but also performs resampling to a standardised *1nm* spectral resolution to allow plotting of both the Rikola and the HR1024i data in a single graph within *ENVI*. Finally, it saves the corrected images into a single image stack.

3.3.2.2 Separability analysis. In order to evaluate whether the Rikola sensor has the potential to distinguish and classify grassland communities related to blaiken, two analysis that determine spectral separability were performed in *ENVI*. These were the JMD and the TDSI, both of which measure the statistical separability between the classes of the chosen areas of interest (shown in Figure 7).

The JMD conveys the probability of the class being separable (Bruzzone, Roli and Serpico, 1995) based on the Bhattacharyya distance (BD) (Magiera, 2017) (Equation 4):

$$BD = \frac{1}{8} * (m_i * m_j)^t \left\{ \frac{\Sigma_i + \Sigma_j}{2} \right\}^{-1} * (m_i * m_j) + \frac{1}{2} \ln \left\{ \frac{|\Sigma_i + \Sigma_j|}{|\Sigma_i| |\Sigma_j|^{\frac{1}{2}}} \right\} \quad (4)$$

with m_i and m_j being the average reflectance values, the two normal distributions i and j and Σ_i , Σ_j , the covariance matrices. BD is then used to calculate the JMD (equation 5):

$$JMD = 2 * \left(1 - e^{-BD} \right) \quad (5)$$

The TDSI is a measure of divergence between classes in a coordinate system. It averages the divergence between all classes and emphasises class distances by means of a weighting system which decreases exponentially with Euclidean distance (Swain and King, 1973; Du et al., 2004). Both indices create values between 0 and 2, whereby class combinations with a value of above 1.9 are considered to have good separability. Both

techniques are specialised on specific aspects of separability. In order to simulate the mixed spectral signature of lower resolution UAV images, the analyses were performed on a down-sampled (bilinear interpolation) image of 100 by 100 pixel, which created a pixel width of approximately 3 cm, similar to the ground sampling size of the UAV footage.

3.3.2.3 Band reduction. When considering bands for grassland classification, the most useful wavelengths are the green (Meyer and Neto, 2008), red, RE and NIR bands (Jensen, 2015), as these bands relay information about pigment content, cell wall properties and water content of plants, which characterize them. Therefore, these bands are present in the most widely used vegetation indexes (Prasad S. Thenkabail, 2016). However, these bands represent a fraction of wavebands when using hyperspectral data. Because of the large number of bands recorded by hyperspectral sensors, it is necessary for most hyper-spectral image analysis to perform band reduction. This process selects the most useful bands for analysis and reduce the data processing workload. *ENVI* software was used for band reduction.

In order to avoid the processing of all 27 bands with approximately 600 images each, the band reduction was conducted on ground images covering the grassland sample areas. They were stitched to one large image and then the the the area outside the sample areas was masked out (Figure 7). The 27 bands were analysed in an R^2 correlation $\lambda_i \times \lambda_j$ matrix, which plots the correlation of each band combination. Identifying clusters of highly correlated bands determined which bands would be the most useful to continue processing (Prasad S. Thenkabail, 2016, p.17). Among band reduction methods, $\lambda_i \times \lambda_j$ R^2 plots are the most popular, due to them retaining reference to the original bands. Thereby biochemical and biophysical attributes can be linked to specific wavelengths and the physical reasons for reactions within each waveband can still be explained (Prasad S. Thenkabail, 2016).

3.3.3 UAV Rikola Data

3.3.3.1 Pre-processing. For the generation of the orthomosaic, only the 7 bands selected from the band reduction analysis were used. The Rikola data from the UAV required the same corrections as the individual images taken on the ground. It also required some further processing to stitch the images to an orthomosaic. This multi-step process is illustrated in Figure 10, which included image selection, point cloud creation, georeferencing, radiometric correction, orthomosaic creation and finally, band stacking and clipping of the image stack. All images captured during the take-off and landing phase, as well those displaying a lot of distortion or warping that the software could not co-register correctly, were manually excluded.

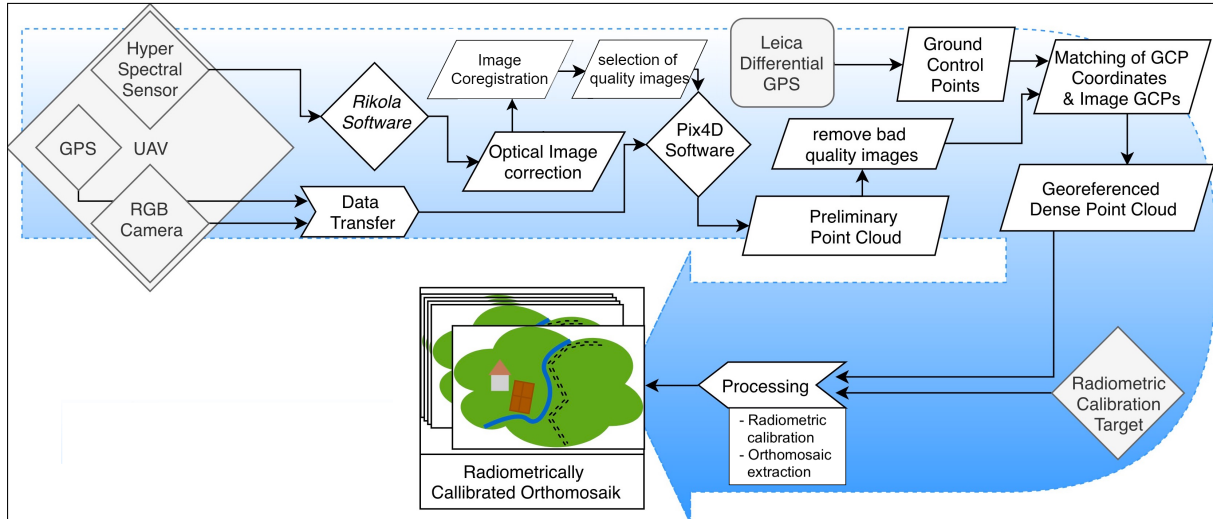


Figure 10: UAV data processing flow chart – The flow chart illustrates the processing workflow from the raw sensor data to the final orthomosaic.

3.3.3.2 Orthomosaic generation, accuracy and resolution. The UAV mounted Rikola camera recorded images every 3 sec during 15 minutes of flying time. Therefore, the number of images during the two flights was around 600 per band. The remaining images, after removing unusable ones, were between 389 and 468 images, depending on the wavelength band. From these images, seven orthomosaics were created; one per selected spectral band. In each process, the images corresponding to the same band were loaded to Pix4D software, together with a table with the UAV GPS coordinates. Locations and images were matched through image capture time and UAV GPS time values. Pix4D then ran an image feature detection algorithm (Structure from Motion) that identifies features in the overlapping parts of the images and tracks them from one image to the next. These features are marked as tie points. These tie points were connected through triangulation and combined to create a 3D dense point cloud (Carrivick, M. W. Smith and Quincey, 2016). Each voxel value (a three dimensional pixel-equivalent in the 3D point cloud) was calculated as an averaged value of all overlapping image pixels. From this point cloud, the software marked images that were not matched and/or the location of which was not able to be calculated. These images were then manually removed from the process. The geometric accuracy of the final orthomosaics, after georeferencing, lies between 0.021 m and 0.051 m root mean square (RMS) error. The average Ground Sampling Distances (GSD) are between 8.59 cm and 9.17 cm. The complete data set being processed consisted of 7 Rikola orthophoto mosaics from bands indicated by Asterix(*) in Table 2. The RGB camera recorded about 1200 images to create the high-resolution RGB orthomosaic. It was created from 716 images and had an accuracy of 0.038 m, with an average GSD of 2.91 cm.

The resulting image extents are illustrated in Figure 11, showing the outer most ortho-

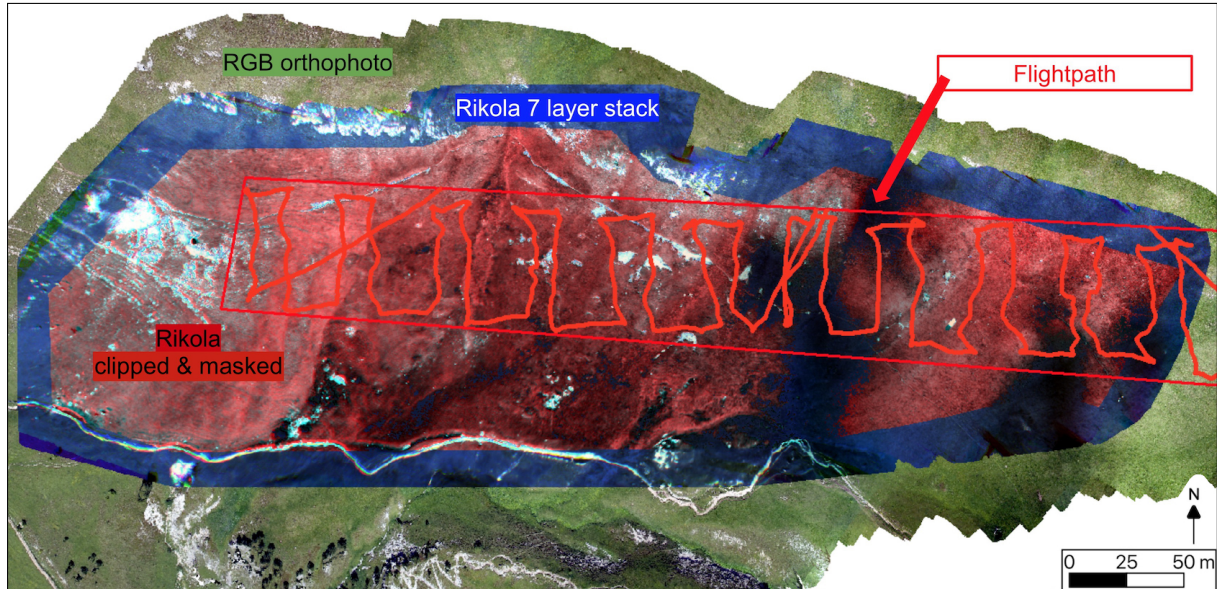


Figure 11: UAV orthomosaic extent – The image illustrates the extent of the final orthomosaics produced from the UAV data. The largest one is the orthomosaic derived from the RGB camera. The two smaller images shaded blue and red for illustration purposes are the hyperspectral orthomosaic in its unchanged form and after it is clipped and masked. (central coordinates: 46°38'12.5"N 11°48'08.3"E)

mosaic that was created with the RGB images. The seven orthomosaics were stacked to a multispectral image and are shaded in blue. This represents the minimum mutual extent of the seven images. As all bands were calculated individually, each image had a slightly different extent. This led to artefacts around the edges. The orthomosaic coloured in red (Figure 11) is a manually clipped version of the original hyperspectral orthomosaic without artefacts, and it also eliminates some colour shifting in the orthomosaic. This colour shifting is evidence of low geometric accuracy of the Rikola bands, occurring in areas far from the flight path. These errors are largest in the areas furthest from the GCPs. The RGB is shown in natural colours while the colours of the multispectral orthomosaics are the result of arbitrary band combination and were chosen solely for illustrative purposes.

Geometric Correction (using GCPs). Pix4D was then used to perform georeferencing. To this end, all five GCP targets were manually identified within the images. As the hyperspectral images have a resolution of 3 cm per pixel, at best, and each layer is monochromatic, it can be challenging to spot and mark the GCP crosses in these images for georeferencing. In order to locate the crosses, a RGB orthomosaic was created from images of the RGB camera, also mounted to the UAV. The images were imported into Pix4D (PIX4D, Lausanne, Switzerland) where the GCPs were manually marked in the images for georeferencing. The resulting high resolution orthomosaic could then be used as a reference map for identifying and locating the GCPs in the bands of the Rikola camera. This was done for as many images as possible and for each band in order to achieve

a high geometric accuracy in the final orthomosaic. In the case of this survey, each GCP was identified within 20 to 100 images (each GCP appears in multiple images). These coordinates allowed Pix4D to re-project the point cloud to the coordinate system of the field GPS coordinates, in this case ETRS 1989 UTM Zone 32N.

Radiometric calibration. When creating an orthophoto, Pix4D asks the user to designate an area within the calibration target and provide its reflectance value. This information is then used to convert the DN values of the image to reflectance values in the final image using the empirical line method (G. M. Smith and Milton, 1999). Fluctuations of the incoming sunlight (irradiance), caused by cloud shadows during the flight, may never be corrected sufficiently and only with great difficulty (Bondi et al., 2016; Milas et al., 2017). Because the calibration of the image requires each pixel be subjected to the same amount of incoming sunlight, different light conditions throughout the scene would negatively impact the calibrated orthomosaic.

The calibration targets can be made of any diffuse reflecting material with known reflectance properties, but preferably one featuring a flat reflectance curve. The reflectance panel in this work was a $2m^2$ sheet of gray synthetic sailcloth with suitable reflectance properties. The exact reflectance properties of the reflectance panel was measured in controlled lighting conditions using the HR1024i spectrometer and the clamp adapter. The HR1024i calibration was performed with spectralon material.

The closest sample areas, which had the most similar light conditions and were expected to have been accurately calibrated, were chosen for comparison with the reference measurements. Due to glare from the the sample area markers caused by strong sun reflection, the orthomosaic sample areas were chosen slightly of-set but close to the grassland sample areas.

In order to find out if the orthomosaic was able to accurately capture the spectral signature of the grassland vegetation, the sample areas' signatures where compared to the reference measurements on the ground. The graph in Figure 12 compares the three spectral signatures (HR1024i, Rikola photos, Rikola Orthomosaic) of the three sample areas, shown as green squares in Figure 6. These are the sample areas (C1, H2, H3) located closest to the UAV calibration targets. Dashed lines represent the signatures taken by the spectrophotometer and show typical vegetation signature forms. The HR1024i signatures do not match up very well with the Rikola ground signatures, especially in the NIR, where there are reflectance differences of up to 20 %. The Rikola signatures taken on the ground should be the most accurate of the three capture methods, as they were calibrated individually with empirical line process (Figure 14) and therefore, do not suffer from light variation, in contrast to the HR1024i instrument, the measurements of which suffered some calibration issues due to changing light conditions. They show typical vegetation

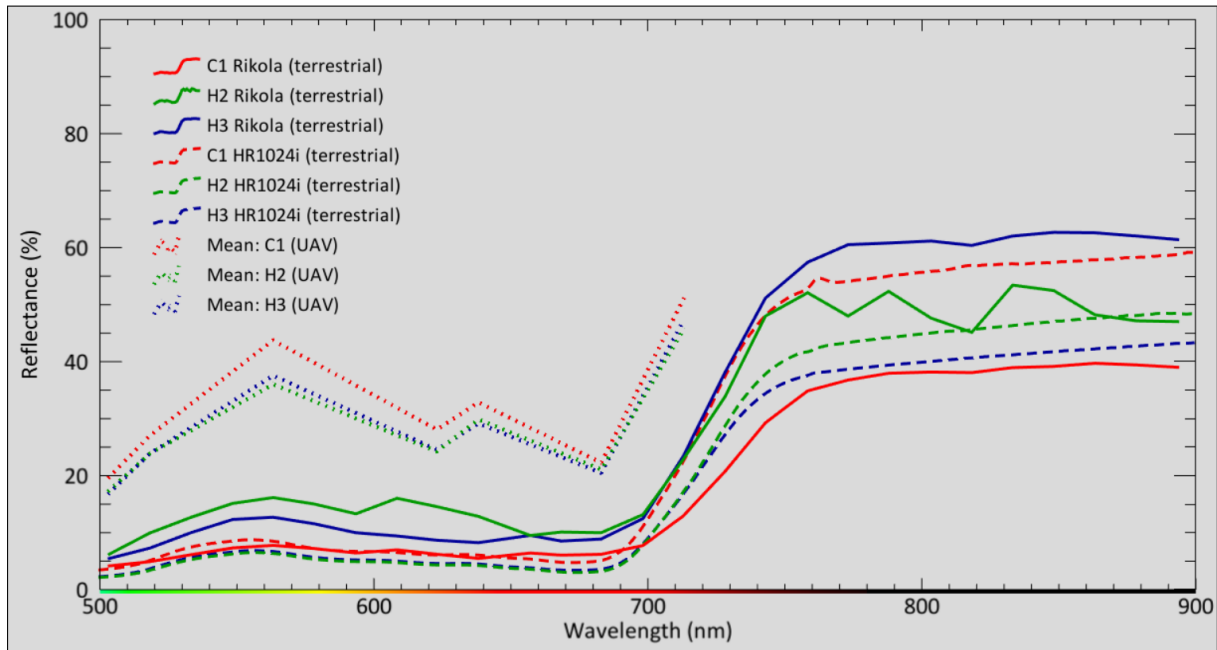


Figure 12: Sample area spectral signatures: Ground vs. UAV – The graph displays the three samples closest to the calibration targets (C1, H2 and H3 indicated as green squares in Figure 6), and therefore most likely to be the best radiometrically calibrated sample areas as the light conditions should have been the most similar to those of the reference area.

spectral curves, with the exception of H2 (mowed pastures), which displays a rugged behaviour, especially in the IR wavelengths. The UAV Rikola measurements, shown as dotted lines, show the signature created from the calibrated seven band orthomosaic. Although somewhat resembling the form of grassland vegetation, they exhibit three to five times higher reflectance values than those recorded by the terrestrial sensors. This increased R is possibly due to glare from the highly reflective sample area bounding boxes. The measurements are also missing three bands in the NIR spectrum due to the sensor failure.

Masking. Cloud shadows are a major disturbance and introduce significant and uncontrollable errors into the data which no current method can totally eliminate. One approach to handle cloud shadows is to mask the areas. Shadow correction methods have also been proposed but can struggle, especially in shadow-light transition zones (Milas et al., 2017). To minimize the cloud shadow interference a 20 class unsupervised *IsoData* classification was calculated in ENVI. This created a map which separated the image into the 20 most spectrally distinct classes. Classes which coincided with visible shadow areas were used to mask out the most severe shadow influences. This unsupervised technique is preferred to a supervised approach, such as the maximum likelihood classification, as supervised techniques tend to include other dark objects such as water bodies (Melesse and Jordan, 2002).

3.3.3.3 Principle component analysis Visual interpretation of the orthomosaic can reveal patterns in the landscape which stand out as being spectrally different. In the process of PCA, new image layers are calculated from multidimensional data by transforming the data into new layers (components). Each component represents the maximum remaining variance within the data and thus the first component holds the highest information content while it decreases for each following component (Prasad S. Thenkabail, 2016). An RGB image is created from the first three components. The components and the RGB image can be useful for analysis and classifications as they often reveal prominent features and important spectral patterns and variations.

3.3.3.4 Normalized difference red edge index The NDRE index is used in order to estimate the vitality of vegetation by measuring chlorophyll content and it is therefore useful for detecting differences in grassland vegetation. It enhances the difference between the red and red edge channels and it is calculated using the Equation 6:

$$NDRE = (red - RE)/(red + RE) \quad (6)$$

, where *red* is the band of the wavelength 682 nm, and *RE* is the band at 712 nm (Dawson and Curran, 1998; Pinar and Curran, 1996). The better known Normalised Difference Vegetation Index (NDVI) is calculated analogous from the wavelengths red (680 nm) and infrared (IR) (800 nm) bands and have been proven to have a strong correlation to vegetation biomass (Goswami et al., 2015). Due to a failure in the IR bands of the Rikola camera, during the flight, the NDRE index was used instead of the NDVI, which requires a NIR band. They both relate very similar information, but while the NDVI is more robust for lower quality data, the NDRE does not saturate as easily when confronted with high biomass and large LAI values and it is superior in monitoring crop variability at later phenological stages with dense vegetation (Sentera, 2018). Moreover, NDRE was also used to mask some non-vegetation classes from the orthomosaic. NDRE values under zero were used to mask out rocks, blaiken and bare soils. Of all vegetation indexes, many lack the red edge or IR spectrum which makes them less robust at separating stressed, dead or dried vegetation from soil (MidOpt, 2019), therefore the NDRE was selected.

3.3.3.5 Separability analysis. In order to measure the grassland classes' potential for classification, the spectral signatures of the sample areas in Rikola's orthomosaic were compared with the spectral signatures of the samples taken with the spectrometer on the ground. ENVI was used to extract the average spectral signature from a $15cm^2$ area of the grassland sample areas in the orthomosaic. Then, separability tests and classifications were performed.

The JMD and TDSI separability scores were calculated for the sample areas in the

UAV orthomosaic. In order to counteract potential shortcomings of either method, the separability was required to be good in both scores to count as providing good separability (*read.ENVI & write.ENVI function* | *R Documentation* 2018). The original plan was to use the area within the square markers as sample areas. However, strong reflection of the square sample markings created a strong glare which influenced the values within. Therefore, similar unaffected areas close to the samples squares were chosen. Here, care also had to be taken in not selecting grassland which had been disturbed during the field work.

3.3.3.6 Maximum likelihood classification. Brenner, Christman and Rogan (2012) suggests maximum likelihood classification in combination with object-based segmentation, when classifying grasslands, which have very similar spectral properties and high within-class variability. This method combination can produce improved results compared to a simple maximum likelihood classification as it also incorporates spatial information. This method was attempted for this research but could not be executed due to multiple failures and errors in creating segmentation in combination with the maximum likelihood method within the available versions of ArcMap, QGIS(QGIS Development Team, open source project) and GrassGIS (mundialis GmbH & Co. KG, Bonn, Germany). Therefore, the maximum likelihood method was performed without the spatial segmentation data.

Based on grassland classes. The same areas used for the separability scores were used to perform the maximum likelihood classification with ArcMap. The maximum likelihood method is a pixel-based statistical approach with a long history in remote sensing and has been used in many studies. While not well suited for individual species classification, the method can reveal patterns and illustrate the abstract values of separability scores and returns accurate predictions for normally distributed data. As the probability of each classes' occurrence was not known an equal probability of occurring within the landscape was assumed (Jensen, 2015). The maximum likelihood method calculates membership values for each pixel, based on the pixels band values, which represent the probability of belonging to a specific class and classifies according to to the highest probability (Frizzelle and Moody, 2001). Disadvantages are its slowness in large datasets and bias for small sample sizes (Ali et al., 2016).

Based on spectral signatures. The visual inspection of the PCA and NDRE index images, as well as knowledge of the area, informed the creation of a reduced set of training areas for a maximum likelihood classification based on four spectrally different regions (pasture and meadow, humid grassland, blaiken area vegetation, rocky grass). PCA and NDRE were calculated in *ArcMap*. 1000 random samples were taken from each training

area for the classification and all pixels from the regions were used for validation and accuracy assessment.

Classification accuracy. The accuracy of the classification was assessed by calculating: 1. total accuracy, 2. kappa value, 3. users' accuracies and 4. producers' accuracies. While the total accuracy determines the percentage pixels that were correctly classified (Congalton, 1991), the kappa value determines how close the class distribution of the classification is to a totally random distribution of classes, with 1 being perfectly classified, 0 being perfectly randomly distributed and -1 being classified completely incorrectly (Congalton, 1991). Producers' accuracy and users' accuracy measure the accuracy of each class from a different perspective (Congalton, 1991). Producers' accuracy measures how much area, which is known to be of a specific class, was correctly classified as that class. The users' accuracy, on the other hand, measures how many pixels, that were classified as a certain class, were actually placed within the correct class areas (validation sample areas).

4 Results

4.1 Relationship of grassland ecology and spatial distribution

Table 3 illustrates the occurrence of different plant species within the sample areas. These are sorted by average proportion over all sample areas. It shows that, on average, the tussock grass *Nardus stricta* is the most frequently occurring species. Other frequent plants are *Bistorta vivipara*, *Leontodon helveticus* and *Trifolium pratense*, which occur in a majority of the sample areas. The areas A (abandoned pasture) and H (mowed pasture) show the highest amount of plant diversity with up to 15 different plant species within each area, while the lowest amount of diversity was found in the grassland areas D (blaiken with little erosion), E (blaiken with strong erosion) and F (humid grassland) with only 4 to 6 different plant types. Overall, it is difficult to ascertain a specific pattern within the data as the botanic classes do not seem to be linked to a particular dominant grassland species. The most abundant grassland species appear only to a small percentage within the classes D (blaiken with little erosion), E (blaiken with strong erosion) and F (humid grassland). The rest of the grassland classes are not dominated by a particular species, but a mixture of many species.

A regression analysis was performed confronting the species abundance vs. distance from blaiken to find out if there is any relationship between grassland types and their occurrence near blaiken erosion spots (Table 3). The highest correlation can be found in *Nardus stricta* and *Arnica montana*. However, the correlation is not significant. Noteworthy species that only occur in areas furthest away from blaiken are *Geum montanum*, *Cisrium spiniosissimum*, *Festuca pulchella*, *Antennaria dioica*, *Salix retusa* and *Soldanella alpina*. Counter intuitively, bare soil only shows in an area the furthest away from the blaiken erosion spots.

Table 3: Plant survey excerpt – Analysis and statistics of 16 grassland sample areas (vegetation classes: Table 1) in the vicinity of blaiken near the Schlüterhütte. This excerpt shows the 9 most abundant plant species in the grassland areas. The rightmost column shows the Pearson’s correlation coefficient. The full table (Table A1) can be found in the appendix. Field survey and species identification conducted by Rita Tonin and Tobias Michael Loebmann from the University of Bolzano)

Plant Species	Vegetation Areas																occ.	avg.	pear. corr.
	A1	A2	A3	B	C	D1	D2	D3	E1	E2	E3	F	G	H1	H2	H3			
<i>Nardus stricta</i>	33	33	20	33	33	20	0	0	0	0	12.5	20	0	20	20	33	11	17.3	0.42
<i>Festuca ssp</i>	0	0	0	0	0	50	33	4	0	0	33	0	0	0	1.5	0	5	7.6	-0.19
<i>Geranium sylvaticum</i>	0	0	0	0	1.5	12.5	50	33	0	0	0	0	0	4	7.5	4	7	7.0	-0.26
<i>Leontodon helveticus</i>	4	4	4	20	0	0	0	0	0	12.5	4	0	33	1.5	1.5	7.5	10	5.8	0.0
<i>Arnica montana</i>	12.5	20	12.5	7.5	0	0	0	0	0	0	12.5	0	0	0	7.5	0	6	4.5	0.68
<i>Alchemilla ssp</i>	0	0	0	0	0	0	0	33	0	0	0	33	0	0	0	0	2	4.1	-0.23
<i>Lingusticum mutellina</i>	4	0	0	7.5	0	0	0	0	0	0	20	12.5	0	12.5	1.5	4	7	3.9	-0.19
<i>Poa</i>	0	0	7.5	4	50	0	0	0	0	0	0	0	0	0	0	0	3	3.8	-0.14
<i>Hormium pyrenaicum</i>	0	0	0	0	0	0	0	0	50	0	0	0	0	0	0	0	1	3.1	-0.15
...																			
Number of Planttypes	10	8	14	9	11	7	4	6	5	7	11	6	9	15	15	10	Correlation between distance and number of Planttypes: 0.387		
Distance from Blaiken (in m)	61.6	47.3	74.9	15.8	3.3	22.1	6.4	12.9	10	1.9	9.9	6.9	20.6	19.6	17.9	23.5			

Additionally, the correlation between distance from the blaiken areas and number of plant species in each grassland area was analysed. Although the values showed moderate correlation, the result was not significantly correlated.

4.2 Spectral analysis at ground level

4.2.1 HR1024i spectral signatures

Figure 13 (a) shows the spectral signatures of the sampled grassland classes recorded with the HR1024i. The spectral signature resembles that typical of vegetation. Lowest values (2–5 %) are visible at 500 nm and 680 nm with a strong increased reflectance of up to 12 % in the green at 560 nm. Sample area F (humid grassland) stands out due to a non-smooth and especially strong reflectance curve between 530 nm and 600 nm, when compared to all other spectra. The red edge is present between 690 nm and 740 nm and ends with a small up or downward spike, present in almost all areas spectra. The IR reflectance values diverge greatly among grassland types, starting with the red edge and ending flat, but slightly increasing after 740 nm. Values in IR range from 36 % to 70 % among sampled grassland areas, but with the same overall progression.

4.2.2 Rikola's spectral signatures from ground level

The spectral signatures as displayed in Figure 13 (b) are calculated from the average reflectance values of the pixels inside of the sample areas (A to H). All signatures display a typical vegetation curve with low reflectance in the visible spectrum, increased reflectance in the green wavelength and a strong increase from 700 nm to 780 nm (red edge). Highest values are found in the IR wavelengths above 780 nm. All areas show this pattern with a very similar progression, especially in the 500–700 nm wavelengths. At longer wavelengths, the areas still display parallel trends but at differing reflectance intensities. Differences of up to 20 % are evident, with the lowest reflectance values in area C (dry grassland) (39 %) and highest in area F (humid grassland) (60 %). The lowest reflectance in all areas occurs near the blue wavelengths at 500 nm (4–6 %). A second minimum occurs at 640 nm. The small reflectance increase observed at 655 nm is not a typical signature for vegetation.

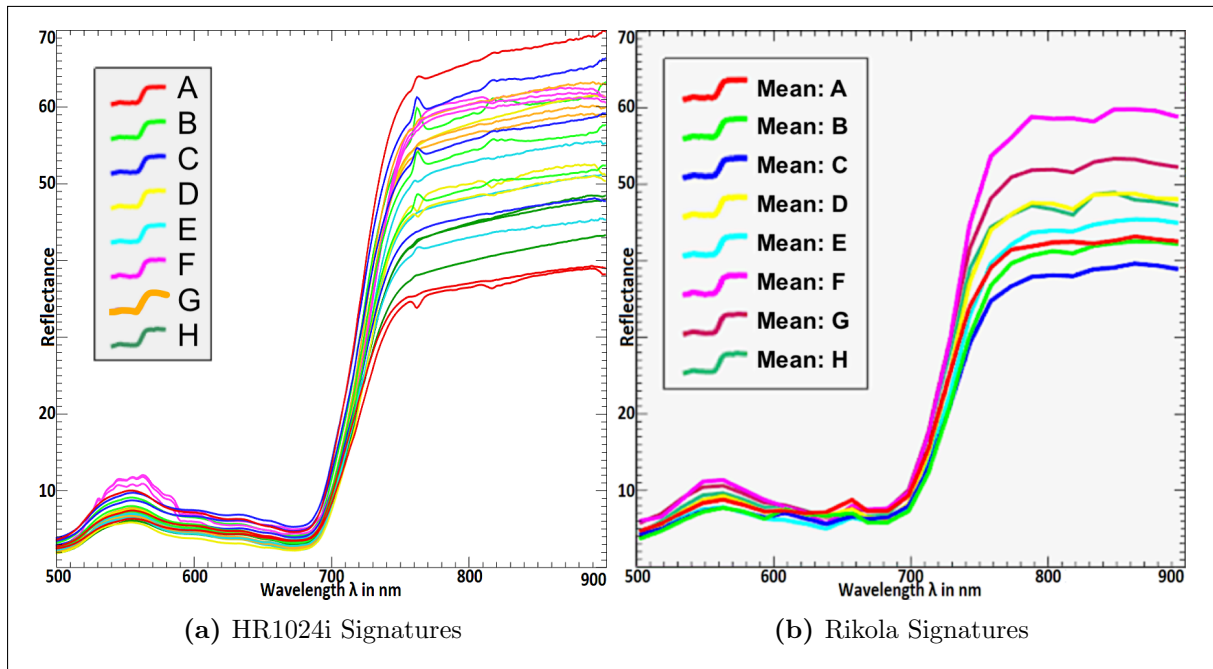


Figure 13: Spectral signatures of sample areas – (a) Spectral signatures recorded by the SVCHR 1024i field radio spectrometer for the sample areas. (b) Averaged Rikola image signatures of the sample areas.

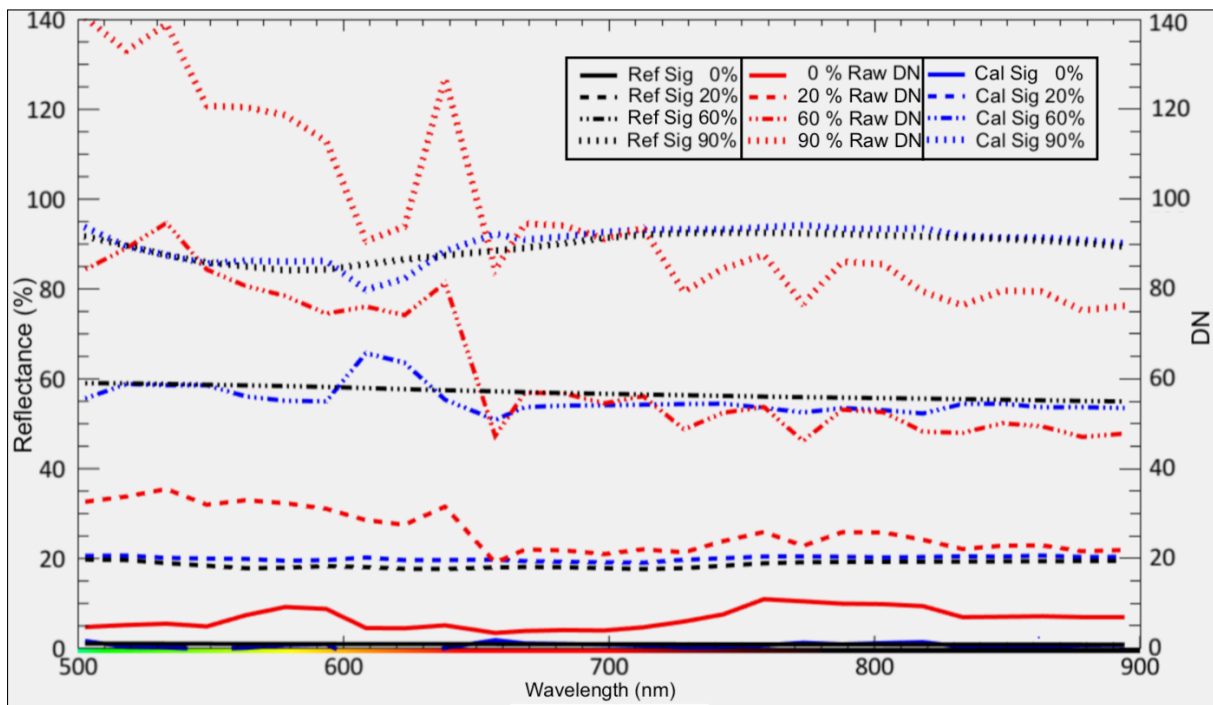


Figure 14: Spectral signatures of calibration targets: Reference, raw DN & calibrated – The reference signature was recorded under controlled and stable artificial light conditions using the HR1024i with a clamp adapter. The raw DN and calibrated signatures are averaged values from the 1010x1010 pixel Rikola camera. The red lines of the raw data are absolute DN values, black and blue are relative reflectance values in %. Therefore DN values can surpass values of 100.

Figure 14 features spectral signatures of the four calibration target cards (0 %, 20 %, 60 %, 90 %) from ground image A1 (abandoned pasture) (Figure 7). The raw Rikola image data is represented in red, the reference reflectance data, recorded by the HR1024i, in black, and the spectral signature from the Rikola camera, after calibration using the empirical line method, is shown in blue. While the uncalibrated values cannot be compared and are highly fluctuating, the blue corrected line shows a high resemblance to the reference curve. The calibrated reflectance values remain within only 2 % of the reference for the majority of the curve. The only issue can be found at the 620 nm wavelength of the 60 % and 90 % calibration targets. Here, the curve deviates +/- 5 % from the reference value.

4.2.3 Spectral separability of grassland classes in ground level Rikola images

The JMD and TDSI are calculated for each image combination at a resolution simulating the Rikola camera at 50 m UAV height (3 cm^2). A value above 1.9 suggests good separability of the classes. Green indicates the class combinations have good separability with scores above 1.9 in JMD as well as TDSI. Table 4 shows the minimum score per class combination and separability test. The highest values are found in class B (natural pasture) and F (humid grassland) vs. most of the other classes. G (pasture) also shows good separability to B (natural pasture), D (blaiken with little erosion) and F (humid grassland). Even the classes that are under the separability threshold of 1.9 usually have high scores close to 1.9. The lowest scores are found in area E (blaiken with strong erosion) with 1.514 and 1.664. F (humid grassland) is the only humid grassland and therefore separates well from the rest of classes. Most of the other classes separate less due to the overall low water content. Pasture area A (abandoned pasture) and B (natural pasture) being of similar vegetation were not expected to be highly separable from each other.

Table 4: Separability between vegetation classes in ground Rikola images – Asterix(*) indicates good separability (minimum score of Jeffries-Matusita and Transformed Divergence algorithm) – a score above 1.9 means good separability (grassland classes: Table 1)

Class	A	B	C	D	E	F	G
B	1.940*						
C	1.751	1.920*					
D	1.806	1.984*	1.896				
E	1.664	1.936*	1.514	1.834			
F	1.982*	1.999*	1.984*	1.937*	1.918*		
G	1.863	1.994*	1.895	1.937*	1.746	1.940*	
H	1.847	1.985*	1.834	1.733	1.986*	1.986*	1.861

4.2.4 Inter- and intra-species spectral differences

Uniqueness of spectral signatures in vegetation communities arise from the varying spectral signatures on the species level. As an example, subsections of a ground Rikola image as well as measurement with the HR1024i clamp adapter were taken of the most abundant species, *Nardus stricta*. The spectral signatures from the Rikola in Figure 15 show typical vegetation signatures and also accurately reproduce the HR1024i signature for *Nardus stricta*. The only inconsistency is displayed in the 660nm wavelength, where the peak is not characteristic of vegetation signatures. The dead or dried specimen displays no green peak, unlike the other samples at 560nm and also display much less reflectance in the IR spectrum. The IR spectrum is very similar to the curve of the shaded *Nardus stricta* specimen. In general, mean values of the healthy plant display little difference in the visible wavelengths while differing up to 20 % in the NIR range. The HR1024i measurement is much smoother due to its higher spectral resolution and reveals a slightly higher reflectance and a shifted green peak at 545 nm in the green wavelengths, while the red and yellow wavelengths are very comparable. Compared to the Rikola values, the HR1024i reflectance values are up to 20 % stronger in the NIR.

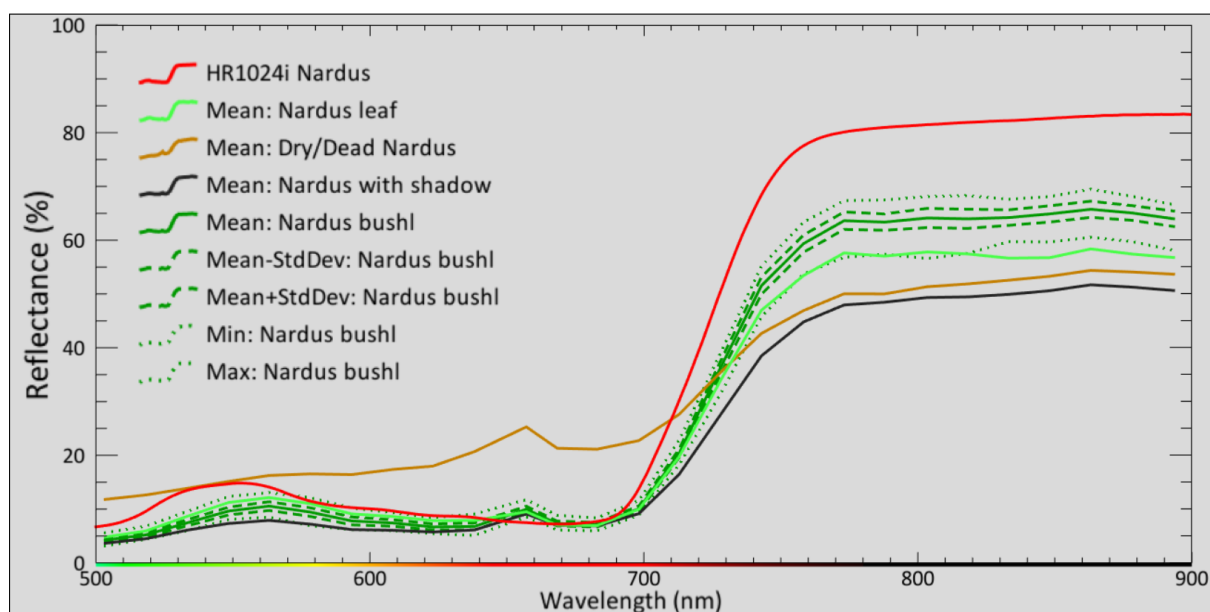


Figure 15: Spectral signatures of *Nardus stricta* – Comparison between various signatures of the Rikola camera and a reference measurement from the spectroradiometer (HR1024i) in red

More effects on spectral signatures are illustrated by light conditions. In Figure 16, leaf signatures were extracted from a Rikola image. The main difference between species is the flat curve of the *Geranium sylvaticum* in the infrared while the *Arnica montana* displays a peak at 780 nm and 810 nm before dropping back to a flat curve at 830 nm.

Differences in light conditions such as shade and leaf angle which causes major differences in the overall reflectance. The graph shows little difference in the visual wavelengths

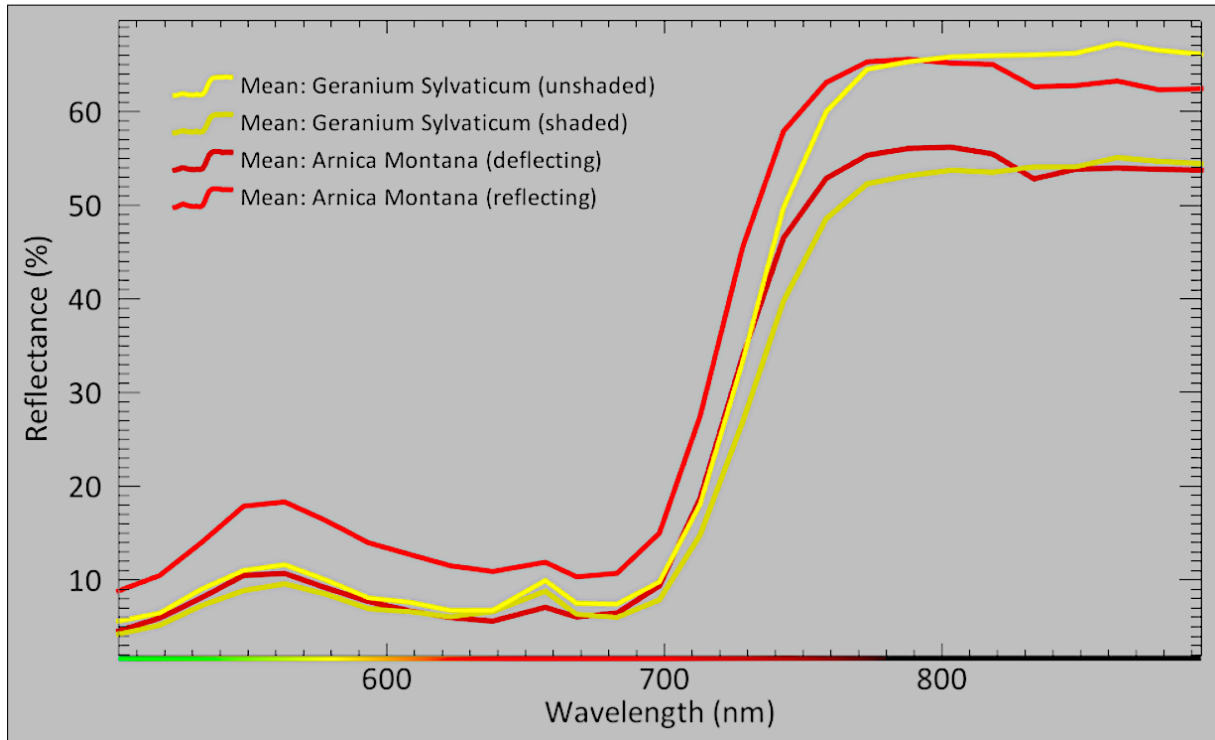


Figure 16: Effect of light conditions on leaf reflectance – The graph shows the spectral signatures of *Geranium sylvaticum* and *Arnica montana* in different light conditions to illustrate the small difference in leaf signature between completely different species as compared to the strong influence of light conditions. The data stems from the Rikola camera

but a strong difference of up to 20%, depending on shade and leaf angle in the NIR spectrum. Also noticeable is the strong increase in the visual wavelengths of 100% at a leaf angle that directly reflects the light to the sensor. In contrast, the reflectance values of unshaded *Geranium sylvaticum* only increase in the NIR spectrum.

4.2.5 Band reduction (Rikola ground images)

In order to optimize the UAV flight, the Rikola photos on the ground were used to select the most relevant bands to detect differences in alpine grasslands. A reduced number of bands is necessary to reduce the integration time of the camera and allows increasing the speed of the UAV. Figure 17 shows a $\lambda_i \times \lambda_j R^2$ matrix for the combined mosaic image of all sample areas. The R^2 correlation for each combination of bands, recorded by the Rikola camera at ground level, is plotted and colour coded to highlight, in green, the bands with the highest degree of correlation, and therefore the most redundant data. λ in Figure 17 refers to the image in a certain

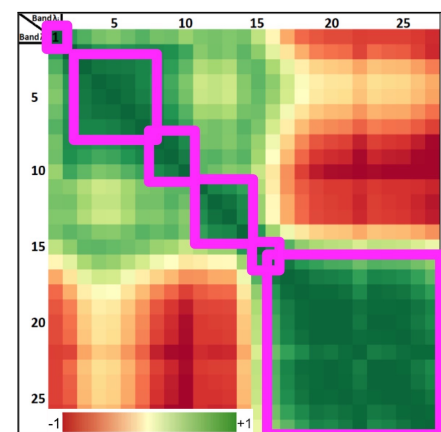


Figure 17: Sample area band correlation – Sample area $\lambda_i \times \lambda_j R^2$ matrix shows the correlation between all bands of the Rikola camera. Red indicates low correlation, green indicates high correlation.

wavelength band ($i = 1, n, j = 1, n$. n is the number of bands (27). It shows the more similar the wavelength, the more similar their information content is. The purple squares outline the areas with a particularly high amount of redundant information. When extracting information from the image, one band (usually the centre) of each square can substitute all other bands within each purple square without losing information. In this case, bands 1, 2, 5, 9, 13, 15, 16, 17 and 27 should be able to achieve similar results as working with all 27 bands.

4.3 UAV data analysis

4.3.1 Spectral separability of grassland classes in UAV orthomosaic

Two separability tests, JM and TD, were performed on the UAV hyperspectral orthomosaics to find out if there was spectral separability between the grassland communities classes defined on the ground by the botanists. Values under 1.9 denote low separability between classes. Table 5 shows the scores of the separability test.

All samples of class A (abandoned pasture) presents a low score as it suffers from underexposure which occurred in the east most regions of the orthomosaic. The sample area B (natural pasture) displays the highest separability scores of between 1.944 and 1.99, although it does have an issue with separating it from class A (abandoned pasture) at a score of only 1.504. G (pasture area) separates from C (dry grassland), A (abandoned pasture), and H (mowed pasture) separates from G (pasture area) and F (humid grassland) from class C (dry grassland). This suggests that least, B (natural pasture), G (pasture area) and F (humid grassland) are good classes for spectral separation. C (dry grassland) and H (mowed pasture) are also good candidates. Most other values fall short of the 1.9 threshold for good separability, which even goes down to 1.031 between classes D (blaiken with little erosion) and H (humid grassland) .

Table 5: Separability between grassland community classes in UAV Rikola images – Red indicates the separability is not good, Asterix(*) indicates good separability (minimum score of Jeffries-Matusita and Transformed Divergence algorithm) – a score above 1.9 means good separability (vegetation classes: Table 1)

Class	A	B	C	D	E	F	G
B	1.504						
C	1.807	1.944*					
D	1.564	1.963*	1.867				
E	1.746	1.992*	1.586	1.339			
F	1.857	1.994*	1.973*	1.616	1.504		
G	1.919*	1.999*	1.965*	1.836	1.137	1.518	
H	1.756	1.953*	1.686	1.031	1.626	1.895	1.987*

4.3.2 Grassland communities map based on botanic classification

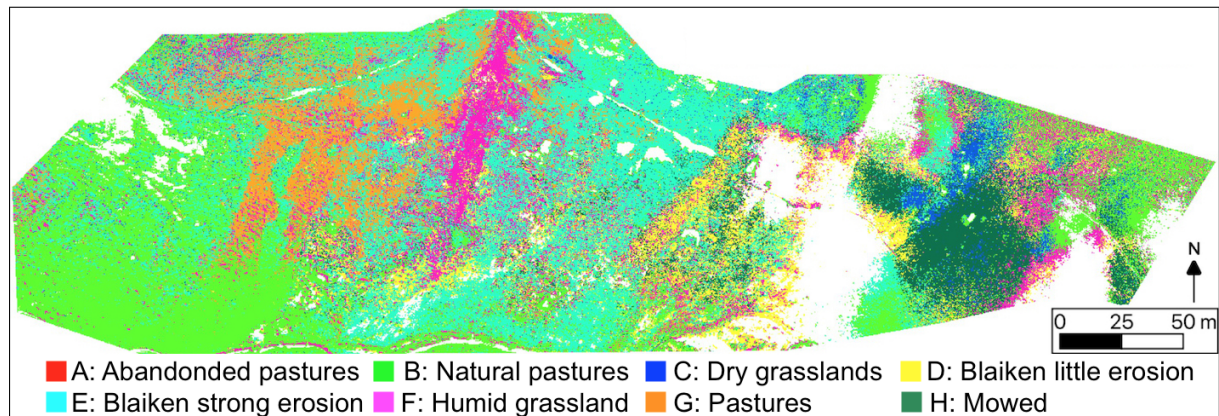


Figure 18: Maximum Likelihood Classification of grassland community classes - (central coordinates: 46°38'12.5"N 11°48'08.3"E) (vegetation classes: Table 1)

Table 6: Accuracy of MLC maps, based on vegetation classes - The table displays the pixel counts of the classes in the grassland communities map and of the classified pixels (grassland type classes: Table 1). The user and producer accuracy percentages state the consensus of class allocation. The total accuracy is a measure of overall accuracy. The Kappa value reflects the randomness of the classification, with 0 being totally random and 1 being perfectly classified (-1 being all pixels were classified wrongly).

Classes	Grassland Type Map Classes								Total	User accuracy	
	A	B	C	D	E	F	G	H			
Classified Pixels	A	38	311	191	7668	2468	775	9106	4596	25153	0.15%
	B	269	32322	1753	23126	14734	9561	30723	13312	125800	25.69%
	C	141	3254	6414	925	10125	2020	3457	7267	33603	19.09%
	D	109	1459	1725	9637	14323	6282	670	7258	41463	23.24%
	E	0	2037	715	37803	31260	21032	15692	4369	112908	27.69%
	F	0	8478	86	5032	1686	29680	7230	5759	57951	51.22%
	G	53	19	5	271	2427	4069	61806	115	68765	89.88%
	H	661	2546	1703	7841	5141	1673	93	34891	54549	63.96%
Pixel in Vegetation Map:	1271	50426	12592	92303	82164	75092	128777	77567	520192		
Producers accuracy	2.99%	64.10%	50.94%	10.44%	38.05%	39.52%	47.99%	44.98%		Total accuracy: 39.61%	
										Kappa: 0.299	

A maximum likelihood classification was performed in order to map the different grassland classes provided by the botanists. Figure 18 displays a maximum likelihood classification map produced from the vegetation sample areas chosen based on their physiologically homogeneous appearance. The classification incorporates all eight classes defined by botanists, of which, the largest areas are covered by category B (natural pasture) in the south west and in small parts in the east, and E (blaiken with strong erosion) in the centre area surrounding most of the blaiken areas. Other large classes can be found west of the central blaiken areas, where the north-south stretching humid area F (humid grassland) is quite accurately classified, as well as the area G to the west of F. Cloud shadows still affect the area east of the blaiken area, where the classification is very messy around the edge of

the cloud mask. Classes A (abandoned pasture) and C (dry grassland) are hardly to be found, as is to be expected due to their sample areas lying in shadows or outside of the orthomosaic. D (blaiken with little erosion) is also absent from most of the scene and can mostly be found in the region contaminated by cloud shadow. The accuracy assessment in Table 6 states a total accuracy of 39.61 % and a kappa value of 0.299. Class A (abandoned pasture) has the lowest accuracy overall (2.99 % and 0.15 %). B (natural pasture) is the class area that was most often predicted correctly (64.1 % of producer accuracy) and class G had the highest percentage of correctly classified pixels (89 % user accuracy).

4.3.3 Grassland communities map based on spectral classes

The spectral separability analysis of grassland types on UAV Rikola orthomosaics revealed that the classes proposed by the botanists were not always separable from a remote sensing point of view. Some classes showed good separability (B: Natural pasture, G: Pasture, and F: Humid grassland) and also C (Dry grassland) and H (Mowed pasture) are good candidates. However, classes A (Abandoned pasture), E (Blaiken with little erosion) and D (Blaiken with strong erosion) were not spectrally separable. Given the nature of these latter classes, it is intuitive that class A (Abandoned pasture) may be merged with class G (Pasture) because of similar management and species composition; while class E (Blaiken with little erosion) should be merged with D (Blaiken with strong erosion), since it is not possible to reach a different classification of blaiken based on intensity of erosion.

Moreover, a visual interpretation of PCA and NDRE images reveals patterns in the landscape which promise to be better suited for classification. The NDRE map (Figure 20) shows values close to 0 in areas such as the rocky grass areas to the north and west, where bedrock shows through the grass surface. NDRE values close to zero denote absence of vegetation, while values close to 1 depict lush green vegetation. Values around 0.5 are in the west and around the blaiken areas in the north-west, center and the convex dry area in the north-east. Grasslands with the highest NDRE values are found in the south, in three north-south and north-west running corridors, and also in the most north-eastern parts. The grassland around the blaiken noticeably shows low to medium NDRE values. There seems to be little to no cloud shadow influence around the masked shadow areas.

The PCA image in Figure 19 reveals four main regions: 1. A turquoise colour in the east represents a pasture area; 2. a healthy, humid grassland displaying in bright turquoise in the three north-south stretching humid areas and in the north-east; 3. blaiken areas are shown in darker green with a red hue in the center and in the convex area in the northeast; 4. rocky grass areas in red/purple to the west, north and some patches in the south; 5. a mixed region around the shadow and in the west, probably abandoned pasture, could not be distinguished from the pasture. The areas to the very west were

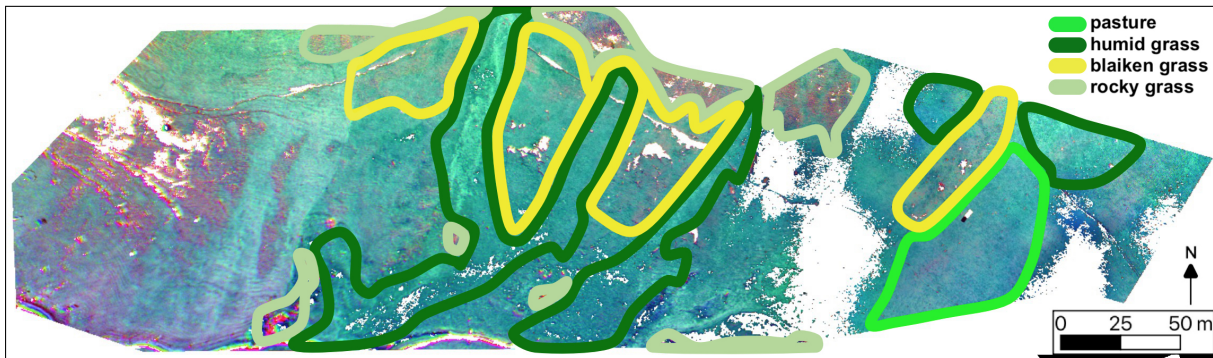


Figure 19: PCA orthophoto (PCA bands 1-3) - (central coordinates: 46°38'12.5"N 11°48'08.3"E)

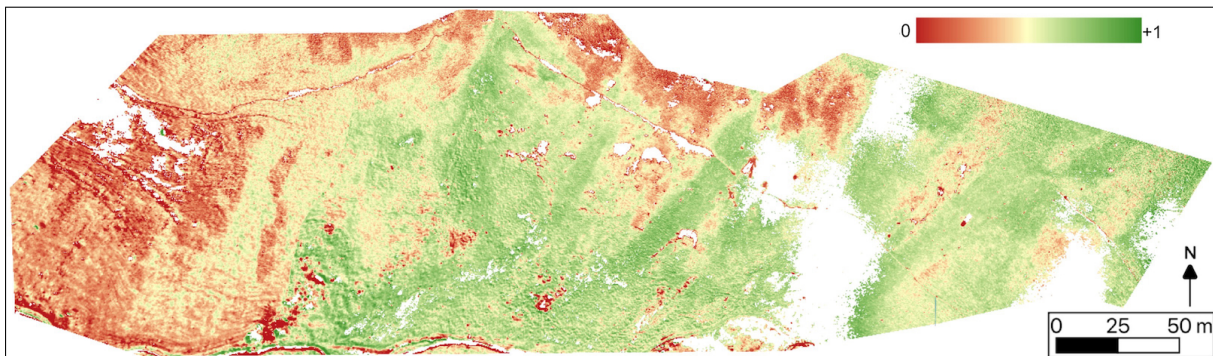


Figure 20: NDRE image of the orthophoto - (central coordinates: 46°38'12.5"N 11°48'08.3"E)

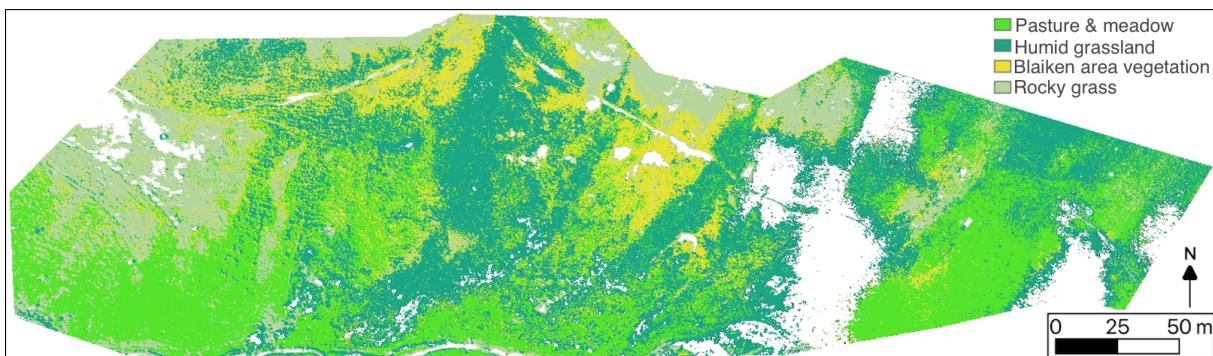


Figure 21: Maximum Likelihood Classification from spectrally distinctive classes - (central coordinates: 46°38'12.5"N 11°48'08.3"E)

Table 7: Accuracy of MLC maps, based on spectral classes - The table displays the pixel counts of the classes in the grassland community map. The accuracy percentages state the consensus of class allocation. The total accuracy is a measure of overall accuracy. The kappa value reflects the randomness of the classification, with 0 being totally random and 1 being perfectly classified (-1 being all pixels were classified wrongly)

Classes	Grassland Community Areas				Total	User accuracy
	rocky grass	humid longgrass area	blaiken area grass	pasture		
Classified Pixels						
Rocky grass	3250	261	2763	43	6317	51.45%
Humid longgrass area	625	6998	1978	571	10172	68.80%
Blaiken area grass	538	300	1053	70	1961	53.70%
Pasture	181	2067	904	3320	6472	51.30%
Pixel in Vegetation Map:	4594	9626	6698	4004	24922	
Producers accuracy:	70.74%	72.70%	15.72%	82.92%	Total accuracy:	58.67%
					Kappa:	0.436

not surveyed so that the vegetation is unknown. The areas marked in Figure 19 denote areas identified by image exploration of NDRE, the PCA, and the authors knowledge of the local circumstances.

Based on the spectral separability analysis, PCA, NDRE and the weak results of the MaxLike map based on botanic classification, a new grassland map was generated, based on spectral classes. The new training areas were chosen and manually drawn into the map. From these areas, 1000 random pixels were used as training samples for the classification. The resulting classification, shown in Figure 21, shows large homogeneous areas of pasture in the south-west and south-east, while also reproducing a transition to unmanaged humid/long grass pasture towards the north. The dark green class marks the humid areas, while also showing up in the cloud shadow area. Based on the authors knowledge of the area, the rocky grass seems to be classified quite accurately, close to the rock formations. Blaiken areas are quite small in comparison to the other classes, but closely trace the locations of the blaiken areas in the north-west and centre. The unknown area in the west was classified as pasture, as was much of the area in the south. The accuracy assessment in Table 7 shows a total accuracy of 58.67 % and a kappa value of 0.436. The most successfully classified classes were pasture and humid grass, with a producers accuracy of 82.92 % and 68.8 % respectively. Only 15.72 % of the assumed blaiken grassland area were classified correctly. However, 53.7 % of all blaiken classifications are found in the corresponding area.

5 Discussion

This thesis investigates the use of hyperspectral imaging in the context of changing agriculture practices and its impact on erosion in the alpine grassland environment. The following section discusses the results and insights of this research. The main research question was, if the orthomosaic from a UAV based hyperspectral camera (Rikola) could succeed in classifying grasslands in an alpine environment with blaiken erosion. To that end, the thesis also explored the radiometric and geometric accuracy of the Rikola hyperspectral camera on the ground and mounted on an UAV.

Despite the UAV Rikola camera not recording the NIR bands, the orthomosaic was able to distinguish some of the grassland types. Compared to the classification based on botanic classes, the classification based on spectral signature patterns had a much better overall accuracy of 58.67 %. This is reasonably good, considering the spectral similarity between the studied classes (Lopatin et al., 2017). It clearly reflects vegetation patterns, especially those seen in the NDRE, such those determined by water content, vegetation cover, vegetation-soil ratio, or vegetation vitality. The rocky grass area, similar to the blaiken erosion area E (Blaiken with strong erosion), closely traces the expected

areas. The map also classifies areas with low species diversity, growing along the blaiken areas. However, this class (blaiken grass) was under-represented in the spectral based classification, as a low producers' accuracy of 15 % shows. In contrast, users' accuracy for this class was over 50 %. This indicates that the training area for blaiken grassland was over estimated and might require the definition of two classes from one of the other classes. The humid vegetation (class F) corridors had the best users' accuracy of all vegetation types. This matches with the good separability predicted by the separability assessment of grassland classes performed on ground Rikola image samples. Also, it aligns with Price (1994), who pointed out that water is a critical discriminating factor for grassland classification. The mowed pasture area (class H) was classified mostly correctly, but was also often wrongly classified as humid grasslands. This suggests that it might be a transition grassland class with intermediate properties associated to water and species composition between classes B (natural pasture) and F (humid grassland).

Spectral signatures acquired with both HR1024i and Rikola photos on the ground of samples for class F (humid grassland) coincided and aligned with typical spectral signatures of vegetation. Both acquisitions had good sampling conditions and therefore indicate the high quality data that is possible to be obtained with the Rikola camera in ideal conditions. The Rikola signatures were proved to be more accurate in practice, due to the line correction method which was shown to be quite robust at ground level and not affected by light conditions that affect UAV flights. The separability analysis of the ground Rikola images showed that separability between classes was possible. However, separability could be further improved by better grassland type definitions that were defined by the botanists, as grassland types defined by species composition and management history were separable only to small degree. The spectral separability responded to some physiological and ecological features of the grassland communities, such as species composition, plant form, vegetation cover, vegetation-soil coverage, humidity and plant vitality.

PCA and NDRE were found to be of great value in the spectral interpretation of the grassland communities. The spectral differences within the orthomosaic were explored through the use of a PCA image (Figure 19). The patterns in the first three principle components coincide with many of the studied grassland classes, such as managed pasture (G) in the east and the humid grassland area (F). Also, the visual inspection of the spectral-based maximum likelihood map depicted a good matching with the grassland classes, as judged by the botanical experts. An NDRE map was also analysed and suggested lower vegetation vitality in the blaiken areas, which might be a precursor or indicator of shallow erosion. Therefore, NDRE might be able to support the prediction of future erosion events. The reduced vegetation cover in blaiken areas is in line with the vegetation surveys, which observed less vegetation diversity and plant density around

the blaiken areas. High NDRE values point to vegetation with higher vitality and clearly reveals the humid grassland corridors in the centre of the scene. Values close to 0 identify areas with little vegetation, such as the rocky grass areas, where the underlying rock occasionally shows through the grass surface. In addition, the NDRE is of special interest, as it seems to be unaffected by cloud shadows. This is probably due to the fact that irradiance is normalised by the index.

While Möckel et al. (2016) and Lopatin et al. (2017) suggest spectral vegetation differentiation should be possible either by species at very high pixel resolution ($< 1\text{cm}$), or by species diversity for slightly lower resolution. The orthomosaic created by the Pix4D software produced a point cloud of 8.59 cm to 9.17 cm GSD. This value is poorer than the expected 6 cm but sufficient for species diversity prediction (Möckel et al., 2016). The spectral signatures in Rikola images show that it was possible to separate the classes. The spectral separability test done on UAV Rikola images of the ground sample areas demonstrated that it was possible to separate the grassland classes. This opens a possibility to create a grassland map showing those types that are more susceptible to blaiken when using the Rikola camera in perfect conditions. Also, the quality of the UAV orthomosaic was not good enough to be used for analysis due to changing light during measurements. The resulting spectral data in our hyperspectral orthomosaic therefore contains highly unreliable reflectance values. The most reliable signatures in our orthomosaic seem to be those of areas G (pasture) and F (humid grassland), as their signatures are the most consistent. The results of the separability test done on the UAV orthomosaic was not as good as that of the ground Rikola image. The class predicted to be most separable was class B (natural pasture), which was only not separable from class A (Abandoned pasture). This could indicate a high similarity between the spectral signatures of classes A (Abandoned pasture) and B (natural pastures). D (Baliken with little erosion) and E are both blaiken afflicted areas and their low separability might be improved by merging them in one single class "Blaiken grassland". The humid grassland class F is separable from the dry vegetation area C (dry grassland) and B (natural pasture). This is because water content is one of the main factors determining spectral signatures in vegetation (Price, 1994). The poor separability results, based on the botanists' classes, reflect the low accuracy scores of the maximum likelihood classification.

The orthomosaic quality was reduced due to some technical and environmental issues such as the malfunction of the sensor, light variation and topographic influences. The underexposure, and therefore loss of images of the NIR waveband was the major issue. This was especially unfortunate, as it was found to be the most distinctive part of the spectrum for the grassland vegetation around blaiken. While the image acquisition of the other bands worked well, clouds interfered strongly with the irradiance during the flight and thereby created problems during the mosaicking process. Cloud shadows were noticeable

throughout the final mosaic and they also influenced the value averaging algorithm of Pix4D when creating the orthomosaic further changing the data to an unknown extent. Some of the areas most affected by shadows were masked out in order to retain the most useful parts of the image.

The successful calibration of the Rikola grassland sample images from the ground, and also other research, such as that by Bareth et al. (2015), has shown that the Rikola camera is capable of accurate spectral capture when mounted to an UAV. Although their fieldwork was over flat ground, homogeneous land cover and only considered a single image Bareth et al. (2015) also experienced handling difficulties. This underlines the difficulty of working with UAV based hyperspectral cameras even without the added complexity of terrain, image mosaicking and similar vegetation. The separation of different vegetation types is much more difficult than separating vegetation from non-green material, especially in an area with a more complex species distribution. Separating different grassland species is even more challenging (Lopatin et al., 2017). Price (1994) showed that mixtures of vegetation can create spectral signatures virtually impossible to distinguish from some reference species, due to the primary factors determining the reflectance values being internal leaf structure, chlorophyll and water content, which are, to a large extent, determined by the immediate and current environmental growing conditions. However, when capturing the spectrum of vegetation communities, these many factors influence on the spectral signature to create a unique signature which is a product of their individual characteristics and their environment. These differences can be witnessed even within a single species when analysed in a hyperspectral image. The spectral mixture can increase the intra-species classification, and thereby improve grassland communities classification. The *Nardus stricta* plant, for example, displays large differences between different plant parts of up to 20 % reflectance, depending on the prevailing biochemical processes and physical properties. The much flatter curve of the dead grass is due to the brown, yellow colour, the reduction of chlorophyll and the loss of reflective capability in the IR spectrum.

Topography and sun angle were also found to have a strong influence on reflectance in satellite images and must be accounted for, especially on steep slopes where it can be a major cause for erroneous classification (Millán et al., 2013). Leaf shading and leaf angle also have an effect on the reflectance values. Reflecting/deflecting position of leaves can have a major effect on the spectral signature. Slope angle and orientation is also a factor which comes into play and affects the reflectance of leaf angles and shading. Effects from topography and sun angle should also be considered for UAV orthomosaics. Though the time of recording (12.00-14.00 o'clock) in June should minimise sun angle effects, the steep slopes of the area will have influenced the results. High classification accuracies were, therefore, not to be expected. Even more so when taking into account the many errors which were introduced along the workflow. The NIR bands were very

useful in separating grassland vegetation in the Rikola photos taken on the ground, but unfortunately the the sensor failed to capture these bands during the UAV flight and could not be used for classifying grassland communities at the map level.

A repeat of the data collection is necessary to take more accurate measurements on a day with better weather conditions and with a fully functioning Rikola sensor. This was planned, but ultimately not possible during the time of the thesis as many of the issues only became evident after considerable time spent on pre-processing and analysis. The effort was additionally hindered by the time required to organise the logistics, the unpredictable weather at the study site and the fast changing phenological stage at this altitude.

5.1 Limitations of the study and recommendations

Although many sources of error influenced the creation of the orthomosaic, it still allowed for the generation of a useful grassland communities map. This section elaborates on other limiting factors of the study and suggests recommendations for future fieldwork.

The moderate accuracy results of the spectral signature based maximum likelihood classification is in part due to the difficulty to separate grassland types, which are very similar spectrally. However, the results are likely to improved with other classification methods and by combining different classification methods. As an example, a study in the flatlands of Schleswig-Holstein implemented a variation of the maximum likelihood classification, more complex than the approach used in this work, which classified similar grassland types (dry grassland, wet grassland, mesophile grassland, intensive grassland and two crop types) and had accuracies of over 89 % (Buck et al., 2015). The results of this study could not achieve as good results due to the lower quality of the data, a larger number of classes and the implementation of the classic maximum likelihood classification method. In combination with other methods, such as object segmentation, accuracy could be further improved. This has been demonstrated by Brenner, Christman and Rogan (2012) who come to the conclusion that a maximum likelihood classification in combination with object-based segmentation can improve results, when classifying grasslands with similar spectral properties and high within-class variability. This is due to it incorporating spatial information.

Our findings also indicate that grassland communities can likely be more accurately mapped with hyperspectral data if the training areas are chosen based on the physiological, environmental and structural properties that define each class and have an effect on the reflectance. This requires a preliminary evaluation of the proposed ground truth samples, and a refinement of the classes, based on the spectral properties of the classes and not only on botanic definition, which might sometimes be unachievable from a remote sensing

approach.

The grassland sample areas at ground level were chosen by randomly throwing square markers in the field. This process should be improved by randomizing locations in a GIS software and locating these location with a GPS. This would also reduce problems with orientation in the field. Additionally, more samples would make the statistics more robust, as sample number between one and three are probably to few.

Some statistical analysis was done on the botanists' plant survey to find a possible relationship of plants and distance to blaiken. Grass, such as *Nardus stricta* has been linked to blaiken areas (Tasser, Mader and Tappeiner, 2003; Wiegand and Geitner, 2010) due their stems, that provoke the accumulation of snow in the winter and therefore pressure blaiken erosion and weak root system, that fails to protect the upper soil layer from water run-off, and. It is probable that lack of grazing has given rise to this type of grass, that does not require such a strong root system to resist the force of grazing animals. However, this study found no significant correlation between plants, species number and blaiken distance. Although there was some correlation found in the data, the sample size was not sufficient to function as contradictory or supporting evidence for the findings of Tasser, Mader and Tappeiner (2003) and Wiegand and Geitner (2010). Our experience in the field supports the idea of a unique plant species composition in the vicinity of blaiken erosion, as also suggested by Tasser, Mader and Tappeiner (2003). Therefore, we think we did our statistic analysis with a low number of samples and if more samples are taken, our results would become reliable. Moreover, we should specifically test the relationship "number of species vs. distance to blaiken" to prove our statement . The humid grass of area F for instance, had a very distinct vegetation with a low species diversity (6 species) as did most of the areas in blaiken vicinity (D and E). *Fetucia spp.* was only found in the blaiken areas. In contrast, the most diverse samples, which show up to 15 different species, were found in the pasture areas A (abandoned pasture) and H (mowed pasture). These areas also had the highest abundance of *Nardus stricta*, which is absent from most blaiken sites. This suggests that a classification based on species diversity could also lead to a useful result, if classes are properly defined.

Further errors can be reduced by flying on an overcast day or cloud-free day at midday (homogeneous light conditions) and multiple slope parallel flights at a uniform height above ground level. It is also important to carry out the flight before the field sampling due to the following contamination (trampling) of the sampling area. A larger sample area marker (50 cm) made from a more suitable material would reduce glare. Topography and sun angle influenced reflectance values strongly. The UAV orthomosaics should therefore be corrected for these effects (Millán et al., 2013). When it comes to the number and distribution of GCPs, this fieldwork utilised around 2 points per 100 images, while Sanz-Ablanedo et al. (2018) suggest at least 3.5 to be ideal.

5.2 Future Research

For future use of the Rikola in an alpine environment, it seems necessary to conduct some research into its capabilities in optimal wind, lighting and different slope conditions, in order to assess the limitations of grassland classification and to understand the implications of slope angle on the spectral signatures. Also, other classification methods might provide better results for mapping grassland and should therefore be tested.

The identification of grassland species related to high and low blaiken erosion risk has been proved to be difficult to do with UAV hyperspectral data; however, this study has found potential in some alternative indicators: 1. the NDRE index revealed low vegetation vitality values around blaiken areas, which might be indicative of future erosion areas. The index's normalisation also reduced radiometric calibration errors due to cloud shadows within the orthomosaic. The incorporation of the NDRE in a workflow for grassland community classification should therefore be investigated in future research. 2. since we observed correlation between the number of species and distance to blaiken, but our results were not significant, a larger number of samples is required for a statistical analysis of this relationship. 3. Species diversity also seems to be potentially related to distance to blaiken, although our results were not significant. It is recommended to continue research of the relationship of species diversity and blaiken erosion.

Previous research for data of the Schlüterhütten area also revealed that not much data is available. The only relatively high quality images are two aerial CIR datasets from 2011 and 2014. In combination with the data acquired during this study and the potential for future data collection with the team's drone, it would be of interest to do time series analysis of the grassland communities in the blaiken areas. Also, existing blaiken areas could be digitalized on aerial images over time, in order to track back "blaiken risk areas". This information can be used to train classifications on older images to test if the classification method is able to predict blaiken erosion before it occurs. Traditionally, classifications require at least two training classes, but this case would only consist of blaiken risk areas and "other" areas. This could therefore be an interesting case study for a one-class support vector machine. One class machine learning classifications are a relatively new field of research in machine learning, which requires only the target class training samples input to be labelled.

6 Conclusion

This research shows that the Rikola camera has the potential to record accurate high-resolution spectral information when used in optimal conditions. Compared to the RGB camera, it is more challenging to produce orthomosaics due to the higher number of images, lower spatial resolution and blur from slow shutter speed. It also requires much more elaborate processing and correction. However, hyperspectral data is the only type capable of separating very similar classes, such as Alpine grassland communities and different grassland management. Therefore, although hyperspectral image analysis is more complex and requires more expertise, it is preferred over more simple remote sensing options, such as RGB and multispectral sensing. It was not possible to accurately separate and classify the grassland communities linked to blaiken in our study area based on botanical criteria only. It was, however, possible to separate some of the grassland classes based on spectral properties of the grassland communities related to physiological and ecological traits, such as vegetation vitality, grassland cover, vegetative forms, vegetation-soil cover ratio or humidity. The relative spectral differences between some grassland types were strong enough to identify and create training samples based on spectral properties which led to a more accurate classification. A further insight resulting from the study is that the species within grasslands are extremely similar from a spectral stand point and that direct classification by spectral signature is difficult. Shading, leaf angle and the environment influence physiological properties of the vegetation, which produces much more intra-species variation in the grassland communities than the potential inter-species differences. The integration of species' signatures within a grassland communities enhances the interspecies differences and is beneficial for the spectral separation of classes. Visual inspection of the NDRE maps and the grassland areas defined by the botanists indicate a possible connection between NDRE values and species richness, as well as a connection between species richness and the distance from blaiken erosion. These observations should be explored statistically in future studies.

Remote sensing research is increasingly focusing on hyperspectral imaging and applications. Satellite Missions such as the Italian PRISMA satellite and the German EnMap mission aim to use hyperspectral information to gain information on geo-, biochemical and biophysical parameters which allow to more precisely describe the dynamics of changes and human impact on ecosystems. This thesis follows along the same lines and facilitated research in the field of shallow erosion dynamics for the EroDyn project. The work demonstrated the potential of UAV remote sensing in an alpine grassland environment with the compact Rikola hyperspectral camera. It also uncovered challenges of this particular remote sensing method, especially when applied in an alpine environment.

References

- Ali, I., F. Cawkwell, E. Dwyer, B. Barrett and S. Green. 2016. Satellite remote sensing of grasslands: from observation to management. *Journal of Plant Ecology* 9.6, 649–671. DOI: 10.1093/jpe/rtw005.
- Autonome Provinz Bozen–Südtirol. 2011. DOLOMITEN WELTERBE UNESCO – Naturparks Südtirol – Naturpark Puez-Geisler. Brochure. From http://www.naturparks.provinz.bz.it/publikation/en.asp?publ_action=4&publ_article_id=985.
- Bareth, G., H. Aasen, J. Bendig, M. L. Gnyp, A. Bolten, A. Jung, R. Michels and J. Soukkamäki. 2015. Low-weight and UAV-based hyperspectral full-frame cameras for monitoring crops. *Photogrammetrie-Fernerkundung-Geoinformation* 2015.1, 69–79. DOI: 10.1127/pfg/2015/0256.
- Berni, J., P. Zarco-Tejada, L. Suárez, V. González-Dugo and E. Fereres. 2009. Remote sensing of vegetation from UAV platforms using lightweight multispectral and thermal imaging sensors. *High-Resolution Earth Imaging for Geospatial Information*. Proceedings of the The International Archives of the Photogrammetry, Remote Sensing and Spatial Information Sciences (Hanover, 2nd–5th June 2009). Germany.
- Blebschmidt, G. 1990. Die Blaikenbildung im Karwendel. *Jahrbuch des Vereins zum Schutz der Bergwelt* 55. [in German], 31–45.
- Blebschmidt, G. 1996. Blaiken formation in the northern Calcareous Alps: an aspect of virtually natural relief formation in high mountain areas, for example the Karwendel Mountains and the Miesbach alpine region. *Geoökodynamik* 17.3-4. [in German, English summary], 271–295.
- Bondi, E., C. Salvaggio, M. Montanaro and A. D. Gerace. 2016. Calibration of UAS imagery inside and outside of shadows for improved vegetation index computation. *Autonomous Air and Ground Sensing Systems for Agricultural Optimization and Phenotyping*. Conference 9866, Paper 9866-17. International Society for Optics and Photonics. DOI: 10.1117/12.2227214.
- Brenner, J. C., Z. Christman and J. Rogan. 2012. Segmentation of Landsat Thematic Mapper imagery improves buffelgrass (*Pennisetum ciliare*) pasture mapping in the Sonoran Desert of Mexico. *Applied Geography* 34, 569–575. DOI: 10.1016/j.apgeog.2012.02.008.
- Bruzzzone, L., F. Roli and S. B. Serpico. 1995. An extension of the Jeffreys-Matusita distance to multiclass cases for feature selection. *Transactions on Geoscience and Remote Sensing* 33.6, 1318–1321. DOI: 10.1109/36.477187.
- Buck, O., V. E. G. Millán, A. Klink and K. Pakzad. 2015. Using information layers for mapping grassland habitat distribution at local to regional scales. *International Journal of Applied Earth Observation and Geoinformation* 37, 83–89. DOI: 10.1016/j.jag.2014.10.012.
- Carrivick, J. L., M. W. Smith and D. J. Quincey. 2016. *Structure from Motion in the Geosciences*. Hoboken: Wiley Blackwell.
- Chang, J. and D. Clay. 2016. Matching Remote Sensing to Problems. *iGrow Corn: Best Management Practices*. Brookings: South Dakota State University, 22 p.
- Cochrane, M. 2000. Using vegetation reflectance variability for species level classification of hyperspectral data. *International Journal of Remote Sensing* 21.10, 2075–2087. DOI: 10.1080/01431160050021303.
- Congalton, R. G. 1991. A review of assessing the accuracy of classifications of remotely sensed data. *Remote sensing of environment* 37.1, 35–46. DOI: 10.1016/0034-4257(91)90048-B.
- Cruzan, M. B., B. G. Weinstein, M. R. Grasty, B. F. Kohn, E. C. Hendrickson, T. M. Arredondo and P. G. Thompson. 2016. Small unmanned aerial vehicles (micro-UAVs, drones) in plant ecology. *Applications in Plant Sciences* 4.9. DOI: 10.3732/apps.1600041.
- Dawson, T. P. and P. J. Curran. 1998. Technical note A new technique for interpolating the reflectance red edge position. *International Journal of Remote Sensing* 19.11, 2133–2139. DOI: 10.1080/014311698214910.
- Du, Y., C.-I. Chang, H. Ren, C.-C. Chang, J. O. Jensen and F. M. D’Amico. 2004. New hyperspectral discrimination measure for spectral characterization. *Optical Engineering* 43. DOI: 10.1117/1.1766301.
- Encyclopædia Britannica. 2018. Grassland. Retrieved 11th Nov. 2018, from <https://www.britannica.com/science/grassland>.
- ERODYN. 2018. ERODYN project website. Retrieved 11th Nov. 2018, from <https://www.mountainresearch.at/erodyn>.

- Fontana, F., C. Rixen, T. Jonas, G. Aberegg and S. Wunderle. 2008. Alpine Grassland Phenology as Seen in AVHRR, VEGETATION, and MODIS NDVI Time Series - a Comparison with In Situ Measurements. *Sensors* 8.4, 2833–2853. DOI: 10.3390/s8042833.
- Frizzelle, B. G. and A. Moody. 2001. Mapping continuous distributions of land cover: A comparison of maximum-likelihood estimation and artificial neural networks. *Photogrammetric engineering and remote sensing* 67.6, 693–706. DOI: 0099-1112/01/6706-693\$3.00/0.
- García-González, R. 2008. Management of Natura 2000 habitats. Alpine and subalpine calcareous grasslands 6170. Tech. rep. Instituto Pirenaico de Ecología, CSIC, Spain.
- Goswami, S., J. Gamon, S. Vargas and C. Tweedie. 2015. Relationships of NDVI, Biomass, and Leaf Area Index (LAI) for six key plant species in Barrow, Alaska.
- Honkavaara, E. and E. Khoramshahi. 2018. Radiometric Correction of Close-Range Spectral Image Blocks captured using an Unmanned Aerial Vehicle with a Radiometric Block Adjustment. *Remote Sensing* 10.2. DOI: 10.3390/rs10020256.
- Ishida, T., J. Kurihara, F. A. Viray, S. B. Namuco, E. C. Paringit, G. J. Perez, Y. Takahashi and J. J. Marciano. 2018. A novel approach for vegetation classification using UAV-based hyperspectral imaging. *Computers and Electronics in Agriculture* 144, 80–85. DOI: 10.1016/j.compag.2017.11.027.
- Jensen, J. R. 2015. Introductory digital image processing: a remote sensing perspective. Upper Saddle River: Prentice Hall Press.
- Labsphere. 2019. Spectralon Targets. Retrieved 11th Nov. 2018, from <https://www.labsphere.com/labsphere-products-solutions/materials-coatings-2/targets-standards/test-child>.
- Leuschner, C. and H. Ellenberg. 2017. Ecology of Central European non-Forest Vegetation: Coastal to Alpine, Natural to Manmade Habitats. Basel: Springer Intl. Publishing.
- Lopatin, J., F. E. Fassnacht, T. Kattenborn and S. Schmidlein. 2017. Mapping plant species in mixed grassland communities using close range imaging spectroscopy. *Remote Sensing of Environment* 201, 12–23. DOI: 10.1016/j.rse.2017.08.031.
- Magiera, A. 2017. Assessment of species composition, productivity and functionality of grassland in the Greater Caucasus (Georgia, Kazbegi Region) by means of remote sensing. PhD thesis.
- Melesse, A. M. and J. D. Jordan. 2002. A comparison of fuzzy vs. augmented-ISODATA classification algorithms for cloud-shadow discrimination from Landsat images. *Photogrammetric Engineering and Remote Sensing* 68.9, 905–912. DOI: 0099-1112/02/6809-905\$3.00/0.
- meteoblue. 2018. Climate Schlüterhütte. Retrieved 3rd Nov. 2018, from https://www.meteoblue.com/en/weather/forecast/modelclimate/schl%C3%BCterh%C3%BCtte_italy_11237553.
- Meusburger, K. and C. Alewell. 2008. Impacts of anthropogenic and environmental factors on the occurrence of shallow landslides in an alpine catchment (Urseren Valley, Switzerland). *Natural Hazards and Earth System Sciences* 8, 509–520. DOI: 10.5194/nhess-8-509-2008.
- Meyer, G. E. and J. C. Neto. 2008. Verification of color vegetation indices for automated crop imaging applications. *Computers and electronics in agriculture* 63.2, 282–293. DOI: 10.1016/j.compag.2008.03.009.
- MidOpt. 2019. NDVI / Agricultural Inspection. Retrieved 21st Feb. 2019, from <https://midopt.com/solutions/color-imaging/ndvi>.
- Milas, A. S., K. Arend, C. Mayer, M. A. Simonson and S. Mackey. 2017. Different colours of shadows: classification of UAV images. *International Journal of Remote Sensing* 38.8-10, 3084–3100. DOI: 10.1080/01431161.2016.1274449.
- Millán, V. E. G., G. A. S. Azofeifa, G. C. Malvárez, G. Moré, X. Pons and M. Yamanaka-Ocampo. 2013. Effects of topography on the radiometry of CHRIS/PROBA images of successional stages within tropical dry forests. *Journal of Selected Topics in Applied Earth Observations and Remote Sensing* 6.3, 1584–1595. DOI: 10.1109/JSTARS.2013.2259471.
- Möckel, T., J. Dalmayne, B. C. Schmid, H. C. Prentice and K. Hall. 2016. Airborne hyperspectral data predict fine-scale plant species diversity in grazed dry grasslands. *Remote Sensing* 8.2, 133. DOI: 10.3390/rs8020133.
- Pinar, A. and P. J. Curran. 1996. Technical Note Grass chlorophyll and the reflectance red edge. *International Journal of Remote Sensing* 17.2, 351–357. DOI: 10.1080/01431169608949010.
- Prasad S. Thenkabail, J. G. L. 2016. Hyperspectral Remote Sensing of Vegetation. Boca Raton: Taylor & Francis. ISBN: 978-143984538-7. DOI: 10.1201/b11222.

- Price, J. C. 1994. How unique are spectral signatures? *Remote Sensing of Environment* 49.3, 181. DOI: 10.1016/0034-4257(94)90013-2.
- read.ENVI & write.ENVI function | R Documentation. 2018. Retrieved 6th Nov. 2018, from <https://www.rdocumentation.org/packages/caTools/versions/1.17.1/topics/read.ENVI%20%26%20write.ENVI>.
- Reubens, B., J. Poesen, F. Danjon, G. Geudens and B. Muys. 2007. The role of fine and coarse roots in shallow slope stability and soil erosion control with a focus on root system architecture: a review. *Trees* 21.4, 385–402. DOI: 10.1007/s00468-007-0132-4.
- Risser, P. G. 1988. Diversity in and among grasslands. Washington DC: National Academy of Sciences.
- Rutherford, G. N., P. Bebi, P. J. Edwards and N. E. Zimmermann. 2008. Assessing land-use statistics to model land cover change in a mountainous landscape in the European Alps. *Ecological Modelling* 212.3-4, 460–471. DOI: 10.1016/j.ecolmodel.2007.10.050.
- Saari, H., V.-V. Aallos, A. Akujärvi, T. Antila, C. Holmlund, U. Kantojärvi, J. Mäkynen and J. Ollila. 2009. Novel Miniaturized Hyperspectral Sensor for UAV and Space Applications. *Proc. SPIE* 7474. DOI: 10.1117/12.830284.
- Sanz-Ablanedo, E., J. Chandler, J. Rodríguez-Pérez and C. Ordóñez. 2018. Accuracy of Unmanned Aerial Vehicle (UAV) and SfM Photogrammetry Survey as a Function of the Number and Location of Ground Control Points Used. *Remote Sensing* 10.10, 1606. DOI: 10.3390/rs10101606.
- Schauer, T. 1975. Die Blaikenbildung in den Alpen. [in German]. Munich: Bayerisches Landesamt für Wasserwirtschaft.
- Schirpke, U., F. Timmermann, U. Tappeiner and E. Tasser. 2016. Cultural ecosystem services of mountain regions: Modelling the aesthetic value. *Ecological Indicators* 69, 78–90. DOI: 10.1016/j.ecolind.2016.04.001.
- Senop Optronics. 2014. VIS-VNIR Snapshot Hyperspectral Camera for UAVs - Manual.
- Sentera. 2018. NDVI vs. NDRE: What's the Difference? Retrieved 21st Feb. 2019, from <https://sentera.com/ndvi-vs-ndre-whats-difference>.
- Simon, R. 1974. RCA electro-optics handbook. RCA.
- Smith, G. M. and E. J. Milton. 1999. The use of the empirical line method to calibrate remotely sensed data to reflectance. *International Journal of Remote Sensing* 20.13, 2653–2662. DOI: 10.1080/014311699211994.
- Spectra Vista Corp. 2012. SVC HR-1024i/SVC HR-768i USER MANUAL–Revision 1.5.
- splinefun function | R Documentation. 2018. Retrieved 6th Nov. 2018, from <https://www.rdocumentation.org/packages/stats/versions/3.5.1/topics/splinefun>.
- Stahr, A. 2014. Blaikentypen. Retrieved 4th Nov. 2018, from <http://www.ahabc.de/wp-content/uploads/2014/07/aha-boden-erosion-mecha-2-800.gif>.
- Stahr, A. and T. Hartmann. 2013. Landschaftsformen und Landschaftselemente im Hochgebirge. Berlin, Heidelberg: Springer-Verlag.
- Swain, P. and R. King. 1973. Two effective feature selection criteria for multispectral remote sensing. *LARS technical reports*, 39.
- Tasser, E., M. Mader and U. Tappeiner. 2003. Effects of land use in alpine grasslands on the probability of landslides. *Basic and Applied Ecology* 4.3, 271–280. DOI: 10.1078/1439-1791-00153.
- Tasser, E., U. Tappeiner and A. Cernusca. 2005. Ecological Effects of Land-use Changes in the European Alps. *Global Change and Mountain Regions*. Dordrecht: Springer, 409–420 p. DOI: 10.1007/1-4020-3508-X_41.
- Themistocleous, K. 2014. The use of UAV platforms for remote sensing applications: case studies in Cyprus. *Second International Conference on Remote Sensing and Geoinformation of the Environment (RSCy2014)*. Vol. 9229. International Society for Optics and Photonics, 92290S. DOI: 10.1117/12.2069514.
- Tucker, C. J. 1979. Red and photographic infrared linear combinations for monitoring vegetation. *Remote Sensing of Environment* 8.2, 127–150. ISSN: 0034-4257. DOI: 10.1016/0034-4257(79)90013-0.
- Väre, H., R. Lampinen, C. Humphries and P. Williams. 2003. Taxonomic Diversity of Vascular Plants in the European Alpine Areas. *Alpine Biodiversity in Europe*. Berlin, Heidelberg: Springer, 133–148 p.
- Von Bueren, S., A. Burkart, A. Hueni, U. Rascher, M. Tuohy and I. Yule. 2015. Deploying four optical UAV-based sensors over grassland: challenges and limitations. *Biogeosciences* 12.1, 163–175. DOI: 10.5194/bg-12-163-2015.

- Wiegand, C. and C. Geitner. 2010. Flachgründiger Abtrag auf Wiesen-und Weideflächen in den Alpen (Blaiken)–Wissensstand, Datenbasis und Forschungsbedarf. *Mitteilungen der Österreichischen Geographischen Gesellschaft* 152. [in German], 130–162. DOI: 10.1553/moegg152s130.
- 2013. Investigations into the distribution and diversity of shallow eroded areas on steep grasslands in Tyrol (Austria). *Erdkunde*, 325–343. DOI: 10.3112/erdkunde.2013.04.03.
- Zweckl, J. and L. Spandau. 1987. Investigations on Blaiken-erosion in the Jenner region of Alpenpark Berchtesgaden. *Landschaft und Stadt* 19.3, 122–128.

Appendices

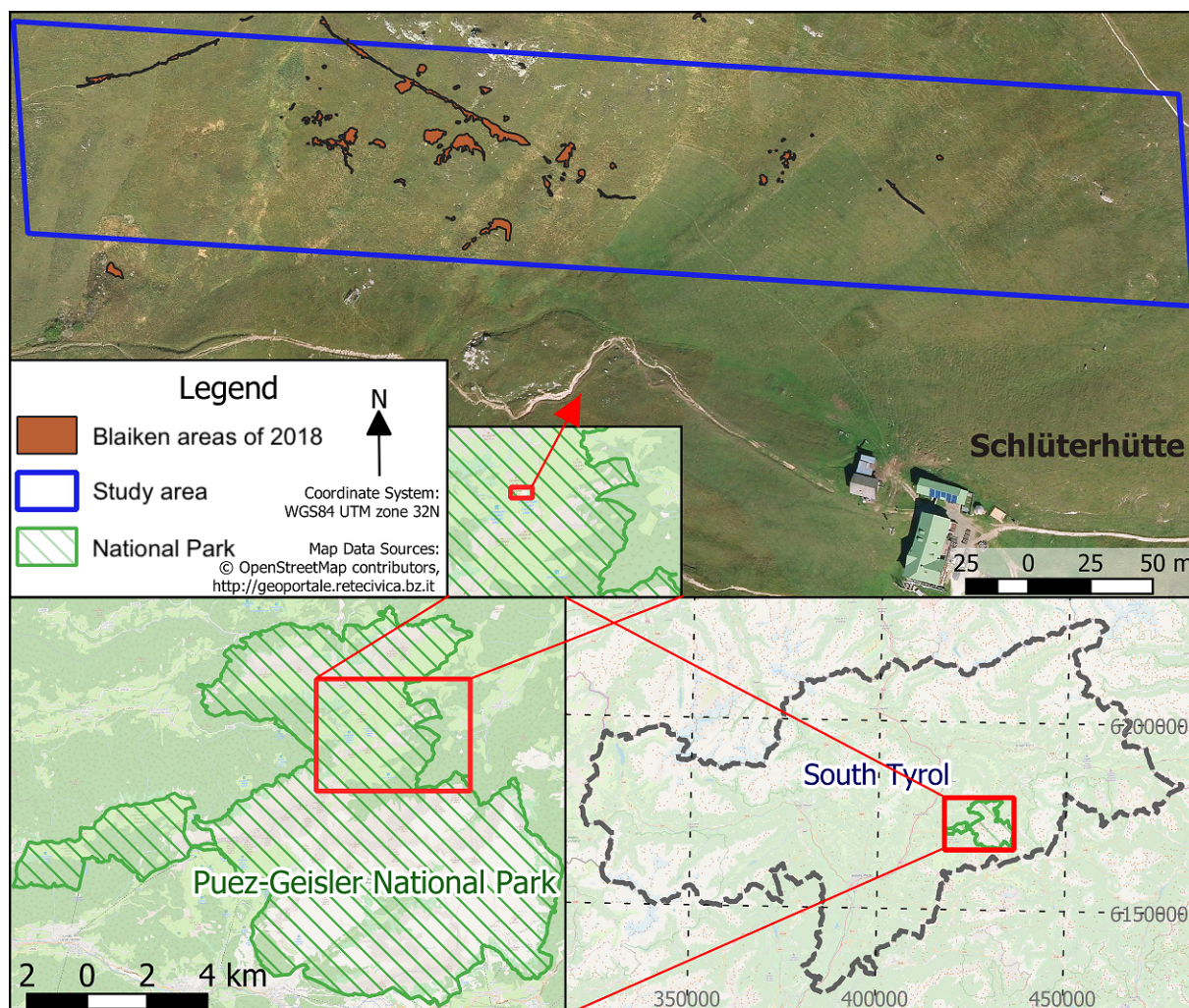


Figure A1: Maps of the study area (large – Location, area of interest & blaiken areas at Schlüterhütte

Table A1: Complete plant survey, Analysis and statistics of 16 vegetation areas in the vicinity of blaiken near the Schlüterhütte. Field survey and identification conducted by Rita Tonin and Tobias Michael Loebmann of the university of Bolzano

Plant Species	Vegetation Areas																occ.	max	avg	pear. corr.
	A1	A2	A3	B	C1	D1	D2	D3	E1	E2	E3	F1	G1	H1	H2	H3				
Nardus stricta	33	33	20	33	33	20	0	0	0	0	12.5	20	0	20	20	33	11	33	17.3	0.42
Festuca sp	0	0	0	0	0	50	33	4	0	0	33	0	0	0	1.5	0	5	50	7.6	-0.19
Geranium sylvaticum	0	0	0	0	1.5	12.5	50	33	0	0	0	0	0	4	7.5	4	7	50	7.0	-0.26
Leontodon helveticus	4	4	4	20	0	0	0	0	0	12.5	4	0	33	1.5	1.5	7.5	10	33	5.8	0.00
Arnica montana	12.5	20	12.5	7.5	0	0	0	0	0	0	12.5	0	0	0	7.5	0	6	20	4.5	0.68
Alchemilla sp	0	0	0	0	0	0	0	33	0	0	0	33	0	0	0	0	2	33	4.1	-0.23
Ligusticum mutellina	4	0	0	7.5	0	0	0	0	0	0	20	12.5	0	12.5	1.5	4	7	20	3.9	-0.19
Poa	0	0	7.5	4	50	0	0	0	0	0	0	0	0	0	0	0	3	50	3.8	-0.14
Horminum pyrenaicum	0	0	0	0	0	0	0	0	50	0	0	0	0	0	0	0	1	50	3.1	-0.15
Potentilla erecta	4	7.5	0	0	4	0	0	0	0	0	0	0	0	12.5	7.5	12.5	6	12.5	3.0	0.15
Sesleria varia	0	0	0	0	0	0	7.5	0	20	0	0	0	20	0	0	0	3	20	3.0	-0.18
Trifolium pratense	0	0	4	12.5	1.5	0.5	7.5	0	0	12.5	0	0	0.5	1.5	4	0	9	12.5	2.8	-0.21
Pulsatilla alpina	0	7.5	12.5	0	4	0	0	0	0	0	20	0	0	0	0	0	4	20	2.8	0.29
Bromus sp	0	0	0	0	0	0	0	0	0	33	0	0	0	0	0	0	1	33	2.1	-0.26
Geum montanum	20	1.5	0	4	0	0	0	0	0	0	0	0	0	0	7.5	0	4	20	2.1	0.47
Ranunculus sp	0	0	0	4	0	0	0	0	0	0	0	20	0	4	4	0	4	20	2.0	-0.22
Bistorta vivipara	1.5	4	1.5	1.5	1.5	0.5	0	0	0	0.5	1.5	0	4	7.5	4	1.5	12	7.5	1.8	0.20
Lotus alpinus	0	0	4	0	0	0	0	0	0	20	1.5	0	1.5	1.5	0	0	5	20	1.8	-0.14
Bare ground	0	20	7.5	0	0	0	0	0	0	0	0	0	0	0	0	0	2	20	1.7	0.54
Homogyne alpina	0.5	0	0	0	0	0	0	0	0	0	0	0	0	0	0	20	2	20	1.3	0.03
Phleum sp	4	0	0	0	0	4	0	12.5	0	0	0	0	0	0	0	0	3	12.5	1.3	0.04
Trollius europaeus	0	0	0	0	0	0	0	0	0	0	12.5	0	7.5	0	0	0	2	12.5	1.3	-0.15
Carlina vulgaris	0	0	0	0	0	0	0	0	0	0	0	0	12.5	4	0	0	2	12.5	1.0	-0.03
Briza media	0	0	0	0	0	0	0	0	0	12.5	1.5	0	0	0	0	0	2	12.5	0.9	-0.28
Helianthemum nummularium	0	0	0	0	0	0	0	0	12.5	0	0	0	0	0	0	0	1	12.5	0.8	-0.15
Polygala alpestris	0	0	0	0	0	0	0	0	12.5	0	0	0	0	0	0	0	1	12.5	0.8	-0.15
Crocus sp	0	0	0	0	0	0	0	0	0	0	0	0	0	4	7.5	0	2	7.5	0.7	-0.06
Carex sp	0	0	0	0	0	0	0	0	0	0	0	0	0	0	7.5	1.5	2	7.5	0.6	-0.05
Cisrium spinosissimum	0	0	7.5	0	1.5	0	0	0	0	0	0	0	0	0	0	0	2	7.5	0.6	0.62
Anthoxanthum alpinum	0	0	0	0	0	4	0	0	0	0	0	0	0	4	0	0	2	4	0.5	-0.02
Deschampsia cespitosa	0	0	0	0	0	0	0	7.5	0	0	0	0	0	0	0	0	1	7.5	0.5	-0.12
Campanula barbata	0	0	0	0	0	0	0	0	0	0	0	0	0	0	7.5	0	1	7.5	0.5	-0.05
Luzula spicata	0	0	0	0	0	0	0	0	0	0	0	0	0	7.5	0	0	1	7.5	0.5	-0.03
Pedicularis tuberosa	0	0	0	0	0	0	0	0	0	0	0	0	7.5	0	0	0	1	7.5	0.5	-0.02
Festuca pulchella	7.5	0	0	0	0	0	0	0	0	0	0	0	0	0	0	0	1	7.5	0.5	0.50
Antennaria dioica	0	0	7.5	0	0	0	0	0	0	0	0	0	0	0	0	0	1	7.5	0.5	0.67
Galium anisophyllum	0	0	0	0	0	0	0	0	0	1.5	4	0	0	0	0	0	2	4	0.3	-0.24
Achillea millefolium	0	0	0	0	1.5	0	0	0	0	0	0	0	0	4	0	0	2	4	0.3	-0.12
Gentiana punctata	0	0	0.5	0	0	0	0	0	0	0	0	0	0	0	4	0	2	4	0.3	0.03
Silene vulgaris	0	0	0	0	0	0	0	0	0	0	0	4	0	0	0	0	1	4	0.3	-0.19
Succisa pratensis	0	0	0	0	0	0	0	0	0	0	0	4	0	0	0	0	1	4	0.3	-0.19
Dead matter	0	0	0	0	0	0	0	0	0	0	0	0	0	0	0	4	1	4	0.3	0.02
Ranunculus acris	0	0	0	0	0	0	0	0	0	0	0	0	0	0	0	4	1	4	0.3	0.02
Aster alpinum	0	0	0	0	1.5	0	0	0	0	0	0	0	0	0	0	0	1	1.5	0.1	-0.24
Fabacea	0	0	0	0	1.5	0	0	0	0	0	0	0	0	0	0	0	1	1.5	0.1	-0.24
Daphne striata	0	0	0	0	0	0	0	0	1.5	0	0	0	0	0	0	0	1	1.5	0.1	-0.15
Succisa pratensis	0	0	0	0	0	0	0	1.5	0	0	0	0	0	0	0	0	1	1.5	0.1	-0.12
Bartsia alpina	0	0	0	0	0	0	0	0	0	0	0	0	0	1.5	0	0	1	1.5	0.1	-0.03
Gymnadenia odoratissima	0	0	0	0	0	0	0	0	0	0	0	0	1.5	0	0	0	1	1.5	0.1	-0.02
Salix retusa	0	0	1.5	0	0	0	0	0	0	0	0	0	0	0	0	0	1	1.5	0.1	0.67
Soldanella alpina	0	0	1.5	0	0	0	0	0	0	0	0	0	0	0	0	0	1	1.5	0.1	0.67
Number of Planttypes	10	8	14	9	11	7	4	6	5	7	11	6	9	15	15	10	Correlation between distance and number of planttypes: 0.387			
Distance from Blaiken in m	61.6	47.3	74.9	15.8	3.3	22.1	6.4	12.9	10.0	1.9	9.9	6.9	20.6	19.6	17.9	23.5				

For each species, the percentage of the ground cover of the plot is given using the following categories:
+ (0.5%); 0.5% (<1%); 1.5%(<2%); 4% (<5%); 7.5 (<9%); 12.5 (15%); 20% (25%); 33% (<40%); 50% (<60%); 80% (<100).
"sp" after the species name means only the Genus but not the exact species could be identified.